Submitted to Journal of Applied Meteorology and Climatology
This version is a non-peer reviewed preprint submitted to EarthArXiv

ENSO, weather regimes, and U.S. heating degree days

Michael K. Tippett,[a] Emily J. Becker,[b] Simon H. Lee,[c] and Michelle L. L'Heureux[d]

[a] *Department of Applied Physics and Applied Mathematics, Columbia University, New York, New York*

[b] *Rosenstiel School of Marine, Atmospheric, and Earth Science, University of Miami, Miami, Florida*

[c] *School of Earth and Environmental Sciences, University of St Andrews, St Andrews, UK*

[d] *NOAA/NWS/NCEP/Climate Prediction Center, College Park, Maryland*

Corresponding author: M. K. Tippett, mkt14@columbia.edu

ABSTRACT: Heating degree days (HDDs; the number of degrees by which average daily temperature falls below 65°F) quantify heating demand and are used to manage weather-related financial risk. Here we examined the relation of El Niño–Southern Oscillation (ENSO) with U.S. cold-season HDDs over the period 1979–2026 in NOAA Climate Division data and observations from stations that are used to settle publicly traded HDD weather derivatives. We focused on monthly resolution to match weather-derivative applications. The strongest ENSO signal is the December decrease in HDDs and HDD variability in the Midwest and Northeast during El Niño. El Niño HDD anomalies are modest in January and reverse sign in November. La Niña signals are weaker overall and consist of HDD increases during late winter and early spring in the Northwest and northern California. These signals are consistent with ENSO modulation of North American weather regime frequency. Pacific Trough frequency increases in December during El Niño, and Pacific Ridge frequency increases in late winter during La Niña, with each weather regime composite resembling the corresponding ENSO one. The station data confirm statistically significant December HDD decreases in Chicago, Cincinnati, and Minneapolis–St. Paul during El Niño and February–March HDD increases in Portland and Sacramento during La Niña. We further quantified these ENSO signals as fair value prices of HDD put options. While the El Niño–La Niña HDD asymmetries are notable, the only statistically significant asymmetry detected here is the December–February variability reduction.

1. Introduction

The 1997–98 El Niño was remarkable both for its record-breaking strength and for occurring at a time when improved scientific understanding, combined with advances in computation and observing systems, made its prediction possible (McPhaden 1999). The El Niño winter of 1997–98 also marked the entrance of weather derivatives as a tool to manage weather risk (Considine 2000). By the middle of 1997, El Niño conditions had developed, and forecasts issued in June of that year called for a moderate to strong El Niño event for the coming winter (Barnston et al. 1999). The economic relevance of this forecast came from the link of El Niño with warmer than average North American winter surface temperatures, which by that time had been well established (Halpert and Ropelewski 1992; Hoerling et al. 1997; Ropelewski and Halpert 1986). Consistent with this expected teleconnection, NOAA/CPC issued a confident forecast in mid-August 1997 for warmer than usual conditions during the coming winter over a broad area of the United States from the northern Plains through the Upper Midwest, Great Lakes, Ohio Valley, and into the Northeast (Barnston et al. 1999). With the expectation of a mild winter, energy utilities and other temperature-sensitive companies looked for ways to reduce their exposure to weather-related risk. Financial markets responded with weather derivatives: insurance-like contracts with payouts linked directly to observed weather outcomes rather than to documented losses. In 1997 Enron was the first firm to offer derivatives based on heating degree days[1] (HDDs), allowing energy utilities and other firms to hedge the financial consequences of an unusually mild winter.

HDDs are the number of degrees by which daily temperature falls below a reference temperature, where daily temperature is defined as the average of a day's maximum and minimum temperatures. The reference temperature, typically 65°F in U.S. applications and 18°C (64.4°F) elsewhere, represents the outdoor temperature below which buildings are assumed to require heating. For instance, a day with minimum and maximum temperatures of 45°F and 67°F has 9 HDDs using the 65°F reference. Summing HDDs over a month or season provides a simple proxy for heating requirements and energy demand (U.S. Environmental Protection Agency 2021). Consequently, HDDs are of particular interest to temperature-sensitive businesses.

An HDD weather derivative is a financial instrument whose payout is based on the observed HDD value at a particular location during a specified period (Campbell and Diebold 2005; Jewson and

[1] "Heating day degrees" would be a less confusing and more accurate description of the quantity being measured.

Brix 2005). The CME Group (formerly Chicago Mercantile Exchange Holdings Inc.) currently offers publicly traded weather derivatives for 13 U.S. cities, four cities in Europe, and one in Asia. The simplest HDD weather derivative is a futures contract whose payout is \$20 for each HDD that occurs. For instance, a Minneapolis–St. Paul HDD futures contract for December 2025 had a settlement value of \$20 × 1430 HDDs = \$28,600. A business whose heating costs are higher during cold weather can offset those costs by buying an HDD futures contract that pays more when a cold winter occurs. HDD options are another type of weather derivative that allows businesses to protect against particular ranges of HDD outcomes. For instance, a put option protects against an unusually mild winter by paying the buyer when the observed HDD value falls below a specified value (called the strike), with the payout increasing the farther the observed HDD falls below the strike. The value of using such weather derivatives comes not so much from their average payout, which might be zero or negative, but rather from reduced year-to-year volatility of costs and earnings.

While ENSO provides a climate context for seasonal temperatures, daily weather with all its complexity determines the HDD values that are actually realized. Weather regime classifications summarize this complexity by grouping synoptic flow patterns into large-scale, physically meaningful, persistent and recurrent circulation states. Weather regimes are well suited for analysis of ENSO and HDDs because prior work with North American regimes has shown that they influence cold-season surface-temperature anomalies and that their frequency is modulated by ENSO phase (Lee et al. 2023; Molina et al. 2023; Pérez-Carrasquilla et al. 2025; Robertson et al. 2020; Straus et al. 2007; Vigaud et al. 2018). Weather regimes have also been linked with regional energy demand and renewable-energy variability in North America and Europe (Rouges et al. 2025; Millin et al. 2024; van der Wiel et al. 2019). Despite the connections between ENSO, HDDs, and weather regimes, notable gaps remain in the scientific literature. First, although the ENSO-HDD relation has been recognized for decades, we are aware of no study that has quantitatively evaluated this relation. Likewise, the relation of weather regimes with HDDs has yet to be formally investigated. There are also secondary gaps. For instance, ENSO impacts North American temperature variability (Becker and Tippett 2024; Martineau et al. 2021; Smith and Sardeshmukh 2000), but the implications of this change in variability on the HDD distribution, which in turn affects option prices, are unknown. Finally, since both ENSO and weather regimes are associated with temperature variability, a natural question is whether the ENSO modulation of HDDs might be expressed through systematic changes in weather regime frequency or intensity (Lee et al. 2023; Straus et al. 2007; Tippett et al. 2024).

Here we addressed some of these gaps. We documented the impact of ENSO and North American weather regimes on U.S. cold-season HDDs using composite analysis. Given the industry emphasis on El Niño impacts, we examined asymmetry in the warm/cool ENSO responses. We assessed the dependence of weather regime frequency and impacts on ENSO phase. We performed spatially resolved analysis to reveal large-scale features, and station-level analysis at the 13 U.S. CME Group weather derivative locations. We computed the fair value price of put options, which are of particular interest in El Niño winters. Data and methods are described in Section 2. Results are presented in Section 3. A summary and discussion are given in Section 4.

2. Data & Methods

a. Data

Our analysis used data from 47 cold seasons: October 1979 through March 2026. Monthly analysis was performed primarily on the five months: November, December, January, February, and March. The station tables and large-scale circulation composites include October. Some seasonal analysis was performed on five overlapping three-month seasons: October–December (OND), November–January (NDJ), December–February (DJF), January–March (JFM), and February–April (FMA).

For spatially resolved analysis, monthly HDD totals for the 344 NOAA Climate Divisions were obtained from the NOAA U.S. Climate Divisional Database (NClimDiv; Vose et al. 2014a), which provides official precomputed divisional temperature and degree-day statistics for the contiguous United States (CONUS). Daily HDDs at the climate division level were computed according to $\mathrm{HDD} = \max(65°\mathrm{F} - T, 0)$ where T is the average of daily maximum and minimum temperatures taken from NOAA nClimGrid-Daily (Durre et al. 2022a), which aggregates gridded daily temperature estimates to NClimDiv divisions. For station-level analysis, we computed HDDs from the average of NOAA GHCND daily TMIN and TMAX for the 13 cities where CME Group weather contracts are offered (Table 1).

TABLE 1: The 13 U.S. cities for which CME Group lists Heating Degree Day (HDD) futures and options, and the GHCND station used for each (NOAA Global Historical Climatology Network-Daily).

City	Station	GHCND ID	Lat (°N)	Lon (°E)
Atlanta	Hartsfield Intl	USW00013874	33.63	−84.44
Boston	Logan Intl	USW00014739	42.36	−71.01
Burbank	Burbank–Glendale–Pasadena	USW00023152	34.20	−118.37
Chicago	O'Hare Intl	USW00094846	41.96	−87.93
Cincinnati	Northern Kentucky Intl	USW00093814	39.04	−84.67
Dallas	Dallas–Fort Worth Intl	USW00003927	32.90	−97.02
Houston	George Bush Intercontinental	USW00012960	29.98	−95.36
Las Vegas	McCarran Intl	USW00023169	36.07	−115.16
Minneapolis–St. Paul	Minneapolis–St. Paul Intl	USW00014922	44.89	−93.23
New York	LaGuardia	USW00014732	40.78	−73.88
Philadelphia	Philadelphia Intl	USW00013739	39.87	−75.23
Portland, OR	Portland Intl	USW00024229	45.60	−122.61
Sacramento	Sacramento Executive	USW00023232	38.51	−121.50

b. North American weather regimes

North American weather regimes were calculated following the year-round method of Lee and Polvani (2026), which is a modification of Lee et al. (2023) that replaced the 10-day Fourier filter by a 5-day centered running mean and that allowed seasonal dependence in trends. The calculation used 500-hPa geopotential height data at 0000 UTC from ERA5 (Hersbach et al. 2020) conservatively regridded to a 1-degree grid over the period 1 June 1979–31 May 2026 with two-day buffers on each end to accommodate the 5-day running mean. There are four regimes: Pacific Trough, Pacific Ridge, Greenland High, and Alaskan Ridge, plus an additional "No Regime" classification representing conditions close to climatology. The cold season (November–March) weather-regime composites are characterized by distinct 500-hPa geopotential height anomaly patterns (Fig. 1). No monthly or seasonal trends in regime frequency are statistically significant after false discovery rate (FDR) control (not shown). The Pacific Trough regime is characterized by an anomalous trough over the Gulf of Alaska and a weaker downstream anomalous ridge over central and eastern Canada, which tends to block the southward advection of cold air. The Pacific Ridge regime features an opposite-sign structure in the northeast Pacific, though otherwise it is not a mirror image of the Pacific Trough. It consists of a strong ridge south of Alaska, negative anomalies over western Canada, and positive anomalies over the eastern United States. This ridge-trough configuration drives cold air southward into western Canada and parts of the western United States, while the downstream ridge brings a warm southerly flow and clear skies to the Southeast. The Greenland High regime is dominated by a broad positive anomaly over Greenland and northeastern Canada, alongside negative anomalies over the western North Atlantic and eastern United States. This configuration is associated with a northeasterly flow into the eastern United States that brings moderately cold temperatures. The Alaskan Ridge regime features a ridge over Alaska and the northeast Pacific, paired with a downstream trough centered over central and eastern Canada. This configuration drives a nearly uniform southward flow directly east of the Rockies, resulting in strong cold air advection into the central United States. See Lee et al. (2023) for further discussion on the robustness of the regime classification and its sensitivity to methodological choices. Geopotential height at 200 hPa was also taken from ERA5 (Hersbach et al. 2020).

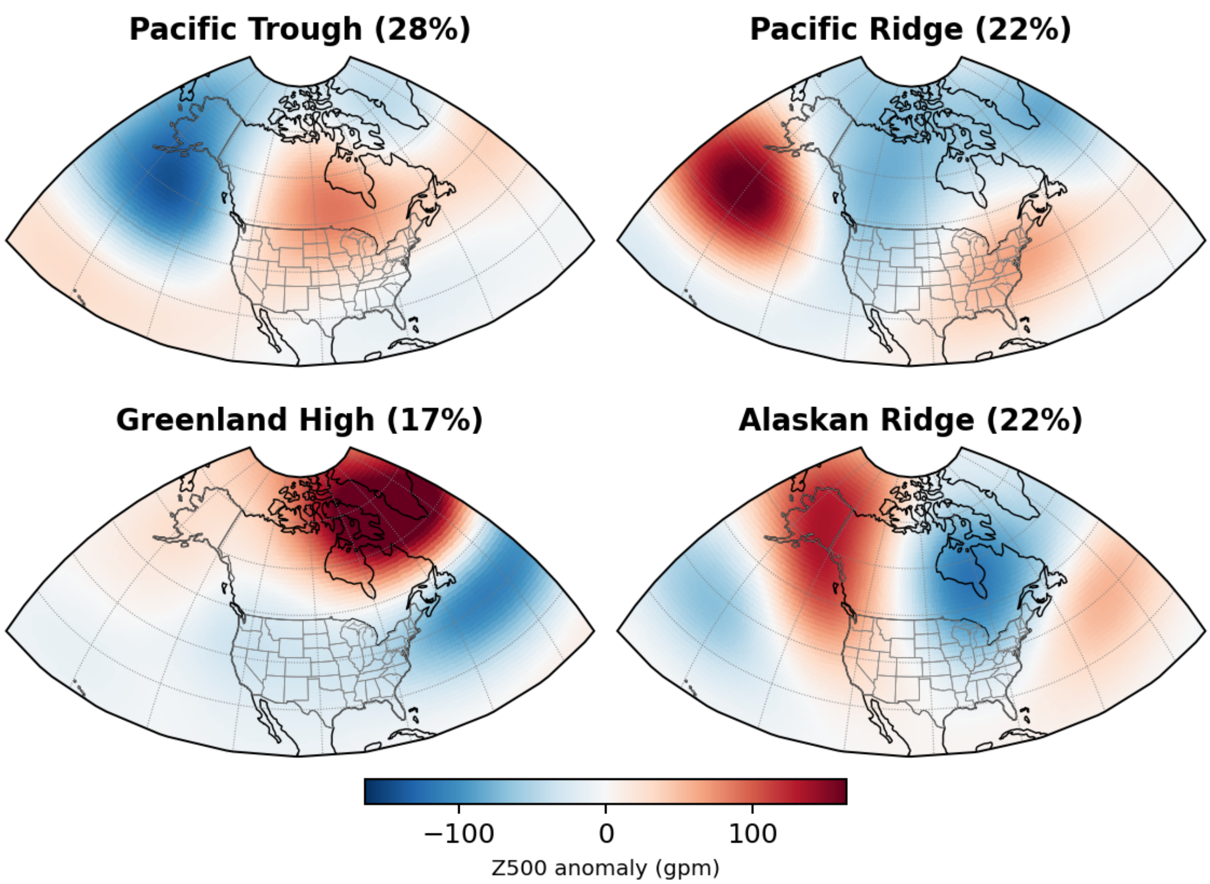

FIG. 1: Cold-season (November–March) detrended 500-hPa geopotential height weather regime composite anomalies. November–March frequencies are shown in the titles.

c. Detrending

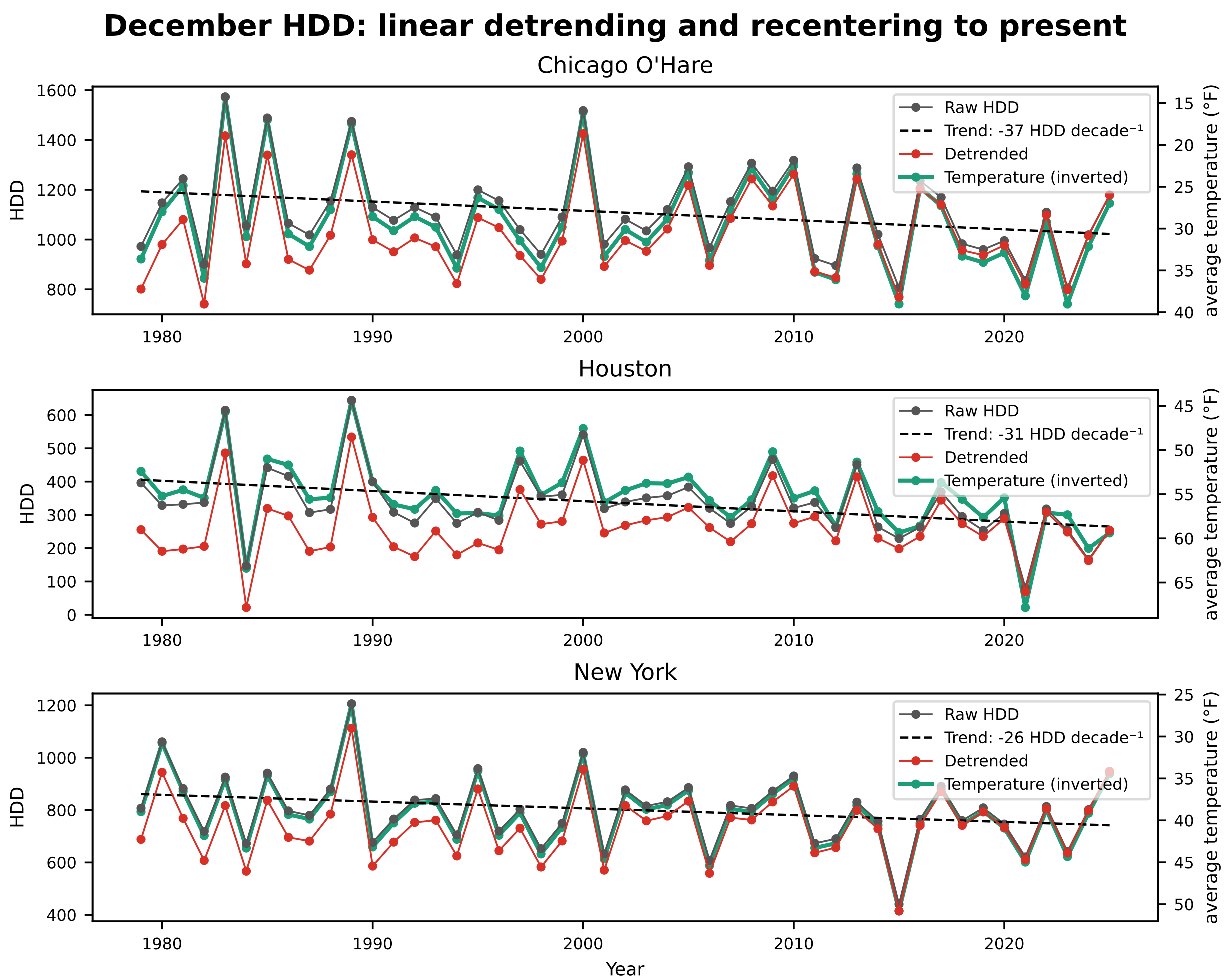

FIG. 2: December raw HDDs, detrended HDDs, and monthly average temperature for Chicago, Houston, and New York. Trend line slope is given in the legend.

HDD data were detrended and recentered to the most recent year using linear regression. Accounting for trends is important because they can affect estimates of ENSO-conditioned climatologies (e.g., Arguez et al. 2019). The recentered value is relevant for HDD derivative pricing and other applications when the total rather than the anomaly is the quantity of interest. Detrending serves to isolate year-to-year variability, and recentering places that variability in the context of the current baseline. Specifically, let $H_{y,m}$ be the number of HDDs at a particular location (grid cell or station) in calendar month m and year y. We fit $H_{y,m}$ with a linear trend:

$$H_{y,m} = \beta_m y + \alpha_m + H'_{y,m},$$

where β_m and α_m are the trend and intercept, respectively, and the residual $H'_{y,m}$ is the detrended anomaly. The recentered (to the most recent year) HDD value $\tilde{H}_{y,m}$ is:

$$\tilde{H}_{y,m} = \beta_m y^* + \alpha_m + H'_{y,m},$$

where y^* is either 2025 or 2026 depending on the month. Figure 2 shows the December values of raw and recentered HDDs for Chicago, Houston, and New York, 1979–2025. The detrended values are shifted lower compared to raw values at the beginning of the period and match them near the end. Inverted monthly average temperature is a close match for raw HDD values because HDD is an affine transformation of the daily temperature when the daily temperature is less than 65°F. Houston shows the largest separation between monthly temperature and HDDs, which reflects the occasional occurrence of mild days there. Other quantities are detrended and recentered in the same manner. For daily data, a single per-month regression was applied.

d. Composite analysis

We quantified ENSO and weather regime impacts using composite analysis. The ENSO phase of each cold season was chosen according to the CPC ONI-based classification of DJF using ERSSTv5, which results in 16 El Niño and 16 La Niña cold seasons. The El Niño winters labeled by winter-end year are: 1980, 1983, 1987, 1988, 1992, 1995, 1998, 2003, 2005, 2007, 2010, 2015, 2016, 2019, 2020, and 2024. The La Niña winters are: 1984, 1985, 1989, 1996, 1999, 2000, 2001, 2006, 2008, 2009, 2011, 2012, 2018, 2021, 2022, and 2023. For instance, the El Niño HDD composite anomaly is the average number of detrended HDDs during El Niño years minus the average number of detrended HDDs during all years. We took the El Niño interquartile range (IQR) anomaly to be the average (over years) of the detrended per-month IQR of daily HDDs during El Niño years minus the same quantity computed over all years.

Statistical significance of the ENSO composite anomalies was assessed using a two-sided permutation test (10,000 permutations of the cold-season year labels). For map quantities, p-values were adjusted for multiple comparisons using the Benjamini–Hochberg false discovery rate (BH-FDR) procedure at $\alpha = 0.10$. We reported the number N_{FDR} of points passing the BH-FDR procedure and the largest p-value among those points, denoted p_{FDR}. The same approach was applied to compute weather regime mean composite anomalies, with averages taken over days in a given regime rather than over years in a given ENSO phase. Weather regime IQR anomalies, in contrast, are pooled quantities: the IQR of the detrended daily HDD values from all days in a given regime (pooled across years) minus the IQR of all days pooled. Pooled IQRs were estimated from 500-bin histograms of the daily values. Statistical significance of the weather regime mean and IQR composite anomalies was assessed with a two-sided block permutation test (10,000 permutations). The permuted block is the regime spell (a maximal run of consecutive same-regime days); each permutation draws, without replacement, as many spells as are observed in the given regime from the pool of all spells in that calendar month or season. ENSO-conditioned weather regime composites were computed by restricting the averages to either El Niño or La Niña years. Within-regime dependence of composites on ENSO phase was quantified as the ENSO-conditioned weather regime composite minus the unconditional weather regime composite. Because the ENSO phase is a property of the whole winter, significance of these composites was assessed by permuting cold-season year labels rather than regime spells.

To motivate our test for asymmetry between El Niño and La Niña responses, consider the linear model for the response Y_i:

$$Y_i = \beta_0 + \beta_{\mathrm{EN}} 1_{\mathrm{EN},i} + \beta_{\mathrm{LN}} 1_{\mathrm{LN},i} + \epsilon_i \,,$$

where the indicator variables $1_{\mathrm{EN},i}$ and $1_{\mathrm{LN},i}$ are one during El Niño and La Niña winters, respectively, and zero otherwise. With this parameterization, the intercept $\beta_0 = \mu_{\mathrm{N}}$ is the neutral-winter mean, while the coefficients $\beta_{\mathrm{EN}} = \mu_{\mathrm{EN}} - \mu_{\mathrm{N}}$ and $\beta_{\mathrm{LN}} = \mu_{\mathrm{LN}} - \mu_{\mathrm{N}}$ are the differences between the El Niño and La Niña means and the neutral-winter mean. The hypothesis that El Niño and La Niña responses are equal in magnitude and opposite in sign therefore corresponds to

$$H_0: \ \beta_{\mathrm{EN}} + \beta_{\mathrm{LN}} = (\mu_{\mathrm{EN}} - \mu_{\mathrm{N}}) + (\mu_{\mathrm{LN}} - \mu_{\mathrm{N}}) = 0 \,.$$

In general, the hypothesis H_0 differs from testing whether the sum of the El Niño and La Niña composite anomalies is zero, because

$$(\mu_{\mathrm{EN}} - \mu_{\mathrm{all}}) + (\mu_{\mathrm{LN}} - \mu_{\mathrm{all}}) = \frac{n_{\mathrm{N}}}{n_{\mathrm{all}}} (\mu_{\mathrm{EN}} + \mu_{\mathrm{LN}} - 2\mu_{\mathrm{N}}) + \frac{n_{\mathrm{LN}} - n_{\mathrm{EN}}}{n_{\mathrm{all}}} (\mu_{\mathrm{EN}} - \mu_{\mathrm{LN}}) \, ,$$

where n_{EN} and n_{LN} are the numbers of El Niño and La Niña events, respectively, and μ_{all} is the all-years mean. When the numbers of events differ, the sum of the composite anomalies contains an additional term proportional to the difference between the El Niño and La Niña means, and differences from zero may reflect that imbalance rather than genuine asymmetry. Here the numbers of events are the same, and there is no distinction. Asymmetry was tested using a three-group bootstrap confidence interval for $\mu_{\mathrm{EN}} + \mu_{\mathrm{LN}} - 2\mu_{\mathrm{N}}$. The bootstrap was used because the asymmetry hypothesis is a linear function of three group means, and the bootstrap resampling directly propagates uncertainty from all three ENSO categories. The test was applied independently at each grid point, and the resulting p-values were adjusted for multiple comparisons using the Benjamini–Hochberg false discovery rate procedure.

e. Put options

The payout of an HDD put option with strike K is $\$20 \times \max(K - \mathrm{HDD}, 0)$, where \$20 is the contract multiplier. We computed the actuarial fair value price $P_{\mathrm{fair}}(K)$ of a put option with strike K as its average historical payout:

$$P_{\mathrm{fair}}(K) = \$20 \times \frac{1}{Y} \sum_{y=1}^{Y} \max(K - \mathrm{HDD}_y, 0) \, , \tag{1}$$

where HDD_y is the recentered HDD value in year $y = 1, \ldots, Y$. The fair value price includes no risk premium or transaction costs; it is the expected payout under the empirical historical distribution. $P_{\mathrm{fair}}(K)$ is a continuous piecewise linear increasing function of the strike K, with slope changes at the observed values of HDD_y. For sufficiently small values of K, the fair value price is zero because no historical HDD value falls below the strike. For K greater than all historical HDD values, the fair value price is equal to \$20 times K minus the average HDD value. The climatological at-the-money

(C-ATM) strike $K_{\text{C-ATM}}$ is defined as the average recentered HDD value,

$$K_{\text{C-ATM}} = \frac{1}{Y}\sum_{y=1}^{Y}\text{HDD}_y = \overline{\text{HDD}}\,.$$

The fair value price of a C-ATM put option measures the variability of HDDs about their mean:

$$P_{\text{fair}}(K_{\text{C-ATM}}) = \$20 \times \frac{1}{Y}\sum_{y=1}^{Y}\max(\overline{\text{HDD}} - \text{HDD}_y, 0)\,.$$

The average lower-tail deviation that appears in the pricing formula is equal and opposite to the upper-tail deviation by construction. If HDDs were equal to their average value in every year, the C-ATM fair price would be zero; deviation of HDDs from their mean increases that price. Put prices conditional on a particular ENSO phase were computed by restricting the sum in Eq. 1 to years in that phase. Confidence intervals were computed by bootstrap resampling years within each sample.

3. Results

a. HDD climatology

The monthly HDD climatology shows the expected strong spatial gradient, with the largest HDD totals in the northern Great Plains, Upper Midwest, and northern New England, and the smallest totals along the Gulf Coast, Florida, and southern California (Fig. 3; top row). In the western United States, the broad north–south HDD gradient is modified by elevation, with the Rocky Mountains appearing as a corridor of locally enhanced HDD totals relative to surrounding lower-elevation regions. HDD totals increase from November into midwinter, peak in January over most of the country, and then decrease through February and March. The seasonal cycle is largest in the northern tier of the United States, where HDD totals exceed 1000 HDD per month in parts of the northern Plains, Upper Midwest, and New England during December–February. The southern United States has much smaller HDD totals and a weaker seasonal cycle, particularly along the Gulf Coast and in Florida, where monthly totals remain comparatively low throughout November–March. The spatial pattern is broadly similar from month to month. The seasonal HDD climatology pattern (Fig. S1; first row) is similar to the monthly one, consistent with the smooth month-to-month variation.

Monthly HDD trends are predominantly negative across most regions and months (Fig. 3; second row). Negative trends are most spatially widespread in December and January, with the largest decreases generally occurring across the central and northern United States. November shows negative trends across much of the western and central United States, while trends over the eastern half of the country are generally weak or near zero. February is the main exception to the overall pattern, with positive HDD trends over parts of the northern and western United States and negative trends over much of the eastern and southern United States. March shows broad negative HDD trends that stretch across most of the country, from the central United States into the Midwest, Southeast, and Northeast. Most monthly trends are not statistically significant after controlling the false discovery rate, with the clearest exception being March, when significant negative trends are widespread. Seasonal HDD trends are predominantly negative and are more often statistically significant than the corresponding monthly trends, with extensive significant negative trends in several three-month seasons (Fig. S1; second row).

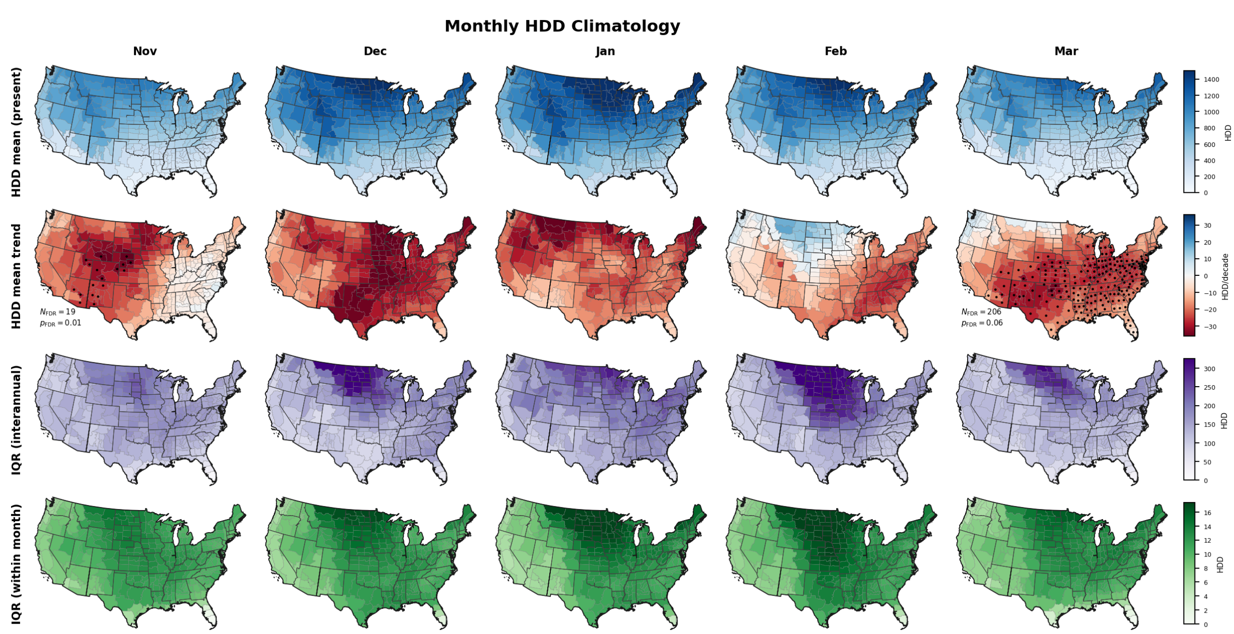

FIG. 3: November–March monthly HDD averages (top row), trends (second row), IQR of monthly averages (third row), and average monthly IQR (bottom row). Dots in the second row indicate trends that are statistically significant after controlling the false discovery rate.

The IQR of monthly mean HDDs shows substantial year-to-year variability in all months, with the largest values generally occurring in the northern Great Plains and Upper Midwest (Fig. 3; third row). The spatial pattern of HDD variability broadly follows from the climatological HDD pattern: regions with larger mean HDD totals in shoulder months tend to have larger interannual variability. February has the largest IQR values, followed by December, especially across the north-central United States, indicating that late and early winter HDD totals vary strongly from year to year. The interannual variability of monthly mean HDDs is large compared with the estimated linear trends. Consequently, even where HDDs have decreased over time, year-to-year variations remain a dominant feature.

In addition to the IQR of monthly mean HDDs, which measures year-to-year variability in monthly totals (Fig. 3; third row), we also computed the mean monthly IQR of daily HDDs, which measures the within-month spread of daily HDD values (Fig. 3; bottom row). This quantity is largest east of the Rockies, especially from the northern Great Plains into the Upper Midwest. Its spatial pattern differs from the mean HDD climatology: the largest within-month daily variability is concentrated over the continental interior rather than simply where HDD totals are largest. February has the largest and most spatially extensive values, with elevated daily-HDD variability extending southward through the central United States. The mean monthly IQR of daily HDDs is modest compared to the IQR of monthly mean HDDs, suggesting that year-to-year shifts of the monthly distribution are large relative to the within-month spread of daily HDD values.

b. ENSO and HDDs

The December El Niño anomaly is the most spatially extensive and statistically significant HDD signal, with widespread negative anomalies from the northern Plains through the Midwest and eastern United States (Fig. 4). Weaker but statistically significant positive HDD anomalies are also present in parts of New Mexico and Arizona. Statistically significant, though less spatially extensive, El Niño HDD anomalies during February are marked by negative anomalies across much of the northern and western United States and positive anomalies along parts of the Southeast and East Coast. January and March have broadly similar anomaly structures to February, with negative anomalies over the northern United States and positive anomalies farther south, but the patterns are weak and not statistically significant after FDR control. In contrast to the expectation of warmer-than-usual conditions, November El Niño HDD anomalies are mostly positive, with the largest values over the southern Plains and adjacent interior West. La Niña mean-HDD anomalies are weaker, less spatially coherent, and not statistically significant in most months. They generally have the opposite sign to the El Niño anomalies. The only statistically significant La Niña HDD anomalies are positive ones over the Pacific Northwest in March. Although the difference between the amplitudes of the El Niño and La Niña HDD composites is notable, the asymmetry is not statistically significant in the monthly composites (Fig. S2).

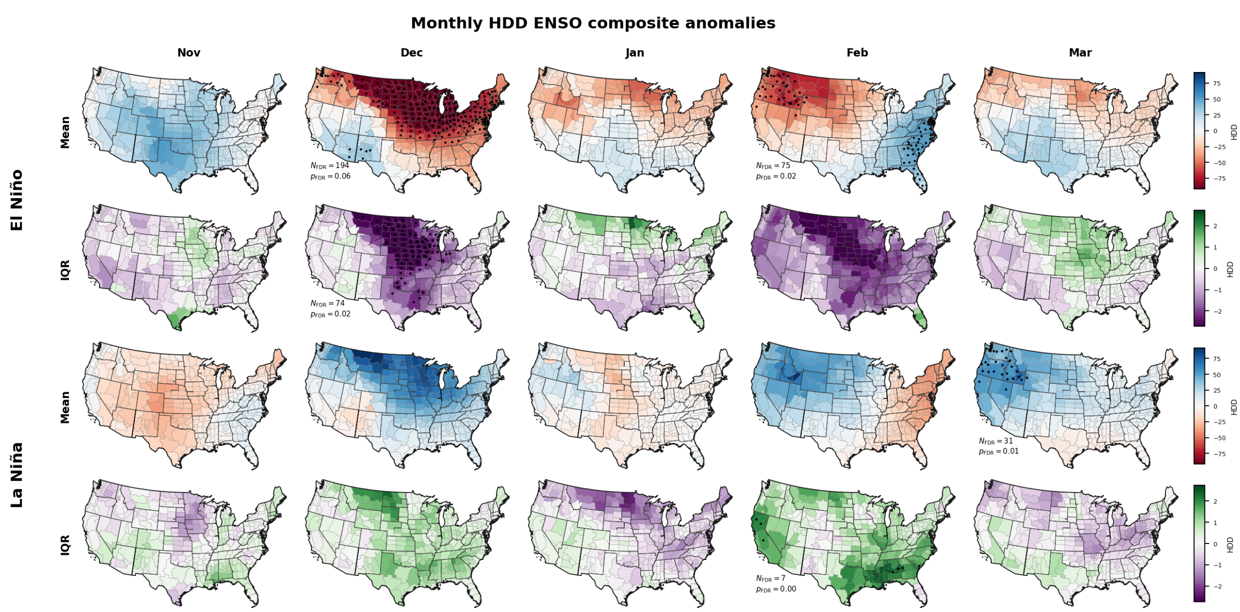

FIG. 4: November–March El Niño HDD composite anomalies (top row) and IQR anomalies (second row). La Niña HDD composite anomalies (third row) and IQR anomalies (bottom row).

El Niño IQR anomalies are large and statistically significant in December, when the within-month spread of daily HDDs is reduced over much of the central United States. February IQR anomalies are nearly as large as those in December, and the lack of statistical significance may reflect the larger climatological variability in February. The El Niño reductions in HDD IQR are consistent with previous work showing reduced daily temperature variability during DJF under El Niño conditions (Becker and Tippett 2024; Smith and Sardeshmukh 2000). La Niña IQR anomalies are most pronounced in February, with increased within-month spread of daily HDDs over parts of California, the Gulf Coast, and the Southeast. The enhanced day-to-day temperature variability along the Gulf Coast and Southeast in February is reminiscent of enhanced severe-weather activity also associated with La Niña conditions (e.g., Cook and Schaefer 2008; Cook et al. 2017).

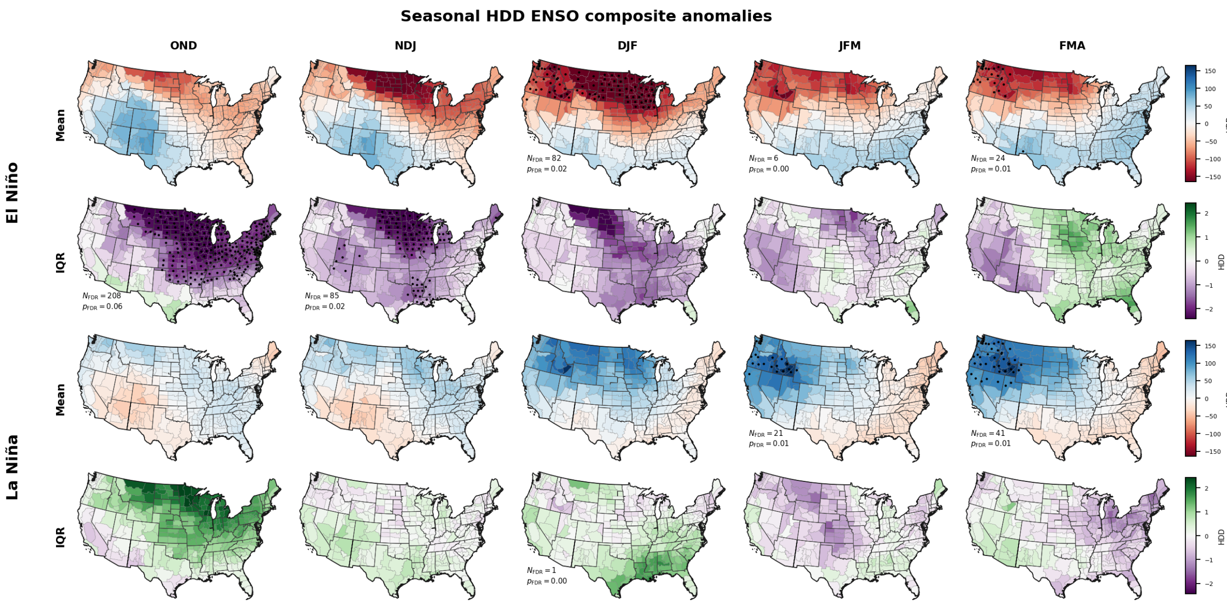

FIG. 5: October–December to February–April ENSO three-month HDD composite and interquartile range (IQR) anomalies.

Three-month seasonal HDD composite anomalies smooth the month-to-month variations (Fig. 5). NDJ and DJF El Niño HDD composite anomalies resemble muted versions of the December composite. The seasonal composites show no indication of the November cooling or the weaker January signal. El Niño IQR reductions are spread across OND, NDJ, and DJF. The El Niño February composite anomaly shows a clear warming in the northwest and cooling in the east that is diluted in JFM and FMA composites. Moreover, the statistical significance is reduced with seasonal averaging. In the La Niña composites, the warming present in November is washed out in the OND and NDJ composites, and the January weakening is no longer visible. Despite the visible differences between the El Niño and La Niña HDD composites, only the DJF IQR asymmetry is significant in the seasonal composites (Fig. S2). We return to the issue of asymmetry in Section 4.

c. Weather regimes and HDDs

The weather-regime HDD composite anomalies are large and spatially coherent across the cold season in three of the four regimes (Fig. 6). The sign and spatial structure of the anomalies vary little with month and are consistent with those previously found for 2-m temperature (Lee et al. 2023). Pacific Trough is associated with negative HDD anomalies centered from the northern Plains into the Upper Midwest, with the strongest anomalies occurring from December through February. The Pacific Trough pattern resembles the December El Niño HDD anomaly, but is present in all cold-season months. Pacific Ridge HDD anomalies have an east–west contrast, with positive values over much of the western United States and stronger negative values over the eastern United States, which are strongest in January. The western positive anomalies during Pacific Ridge are qualitatively consistent with the late-winter La Niña HDD signal. Greenland High HDD anomalies are positive in all months, but only strong and statistically significant in January. Alaskan Ridge is associated with strong, widespread positive HDD anomalies centered over the northern Plains, Upper Midwest, Great Lakes, and northeastern United States. In addition, there are modest negative HDD anomalies in parts of California and Oregon. These also broadly match the probability of severe cold-air outbreaks in Lee et al. (2019), who noted that extreme United States cold was essentially absent in the Pacific Trough regime while Alaskan Ridge was the main driver of extreme cold.

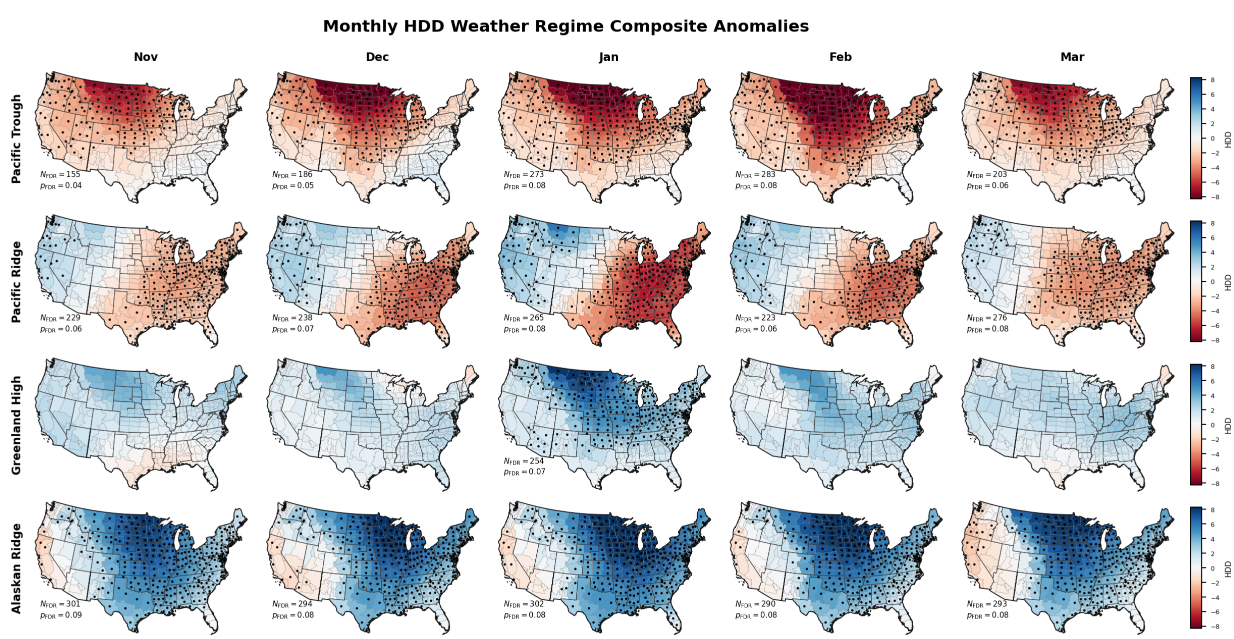

FIG. 6: November–March Pacific Trough, Pacific Ridge, Greenland High, and Alaskan Ridge per-day HDD composite anomalies.

Weather-regime effects on daily-HDD variability are less coherent than the corresponding effects on mean HDD (Fig. 7). Reduced within-month daily-HDD variability from December through February during Pacific Trough days is the clearest signal. This Pacific Trough IQR reduction pattern resembles the December El Niño one, extending the similarity between December Pacific Trough and El Niño HDD responses to include variability. IQR anomalies associated with the other weather regimes are weaker and less consistent across months.

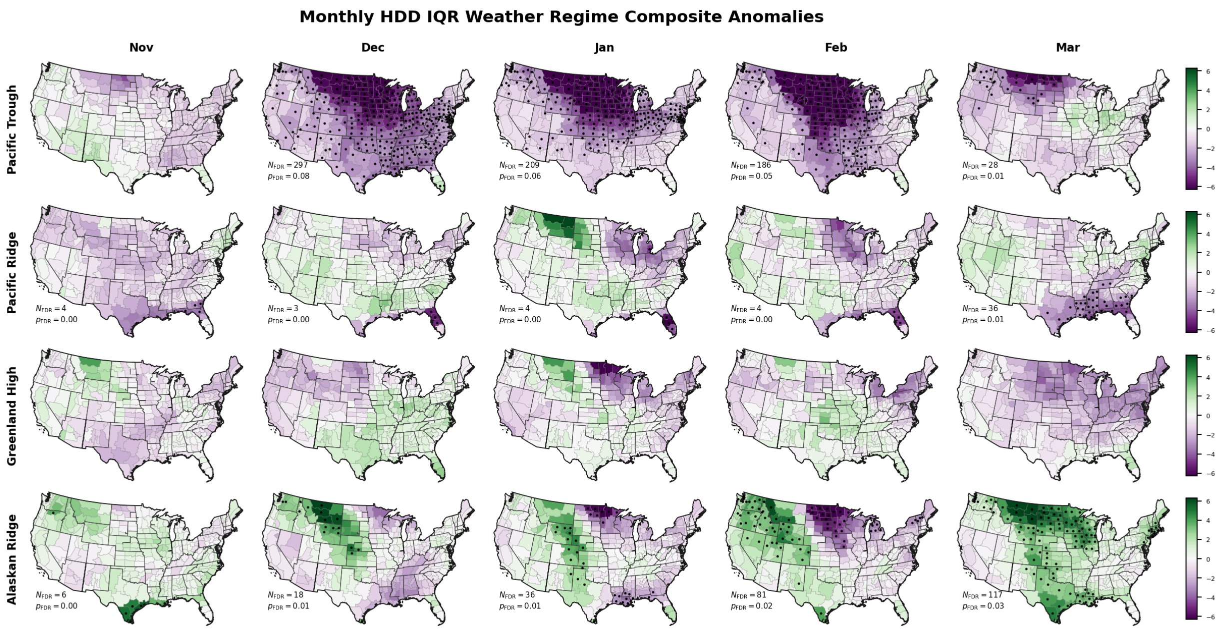

Fig. 7: November–March Pacific Trough, Pacific Ridge, Greenland High, and Alaskan Ridge daily HDD IQR composite anomalies.

d. ENSO and weather regimes

To address the question of whether the ENSO relation with HDDs is expressed through weather regime changes, we checked whether ENSO changes either weather regime intensity or frequency. For the question of weather regime intensity, we computed the within-regime dependence of composites on ENSO phase (Figs. S3, S4). Overall, there is a tendency for the within-regime HDD anomalies to be negative for El Niño and positive for La Niña, consistent with the El Niño tendency toward reduced HDDs and that of La Niña toward HDD increases. Despite these within-regime differences, only one of the within-regime anomalies is statistically significant after controlling the false discovery rate: the December Alaskan Ridge anomaly during El Niño (fewer HDDs over the Midwest and East and more over the Southwest).

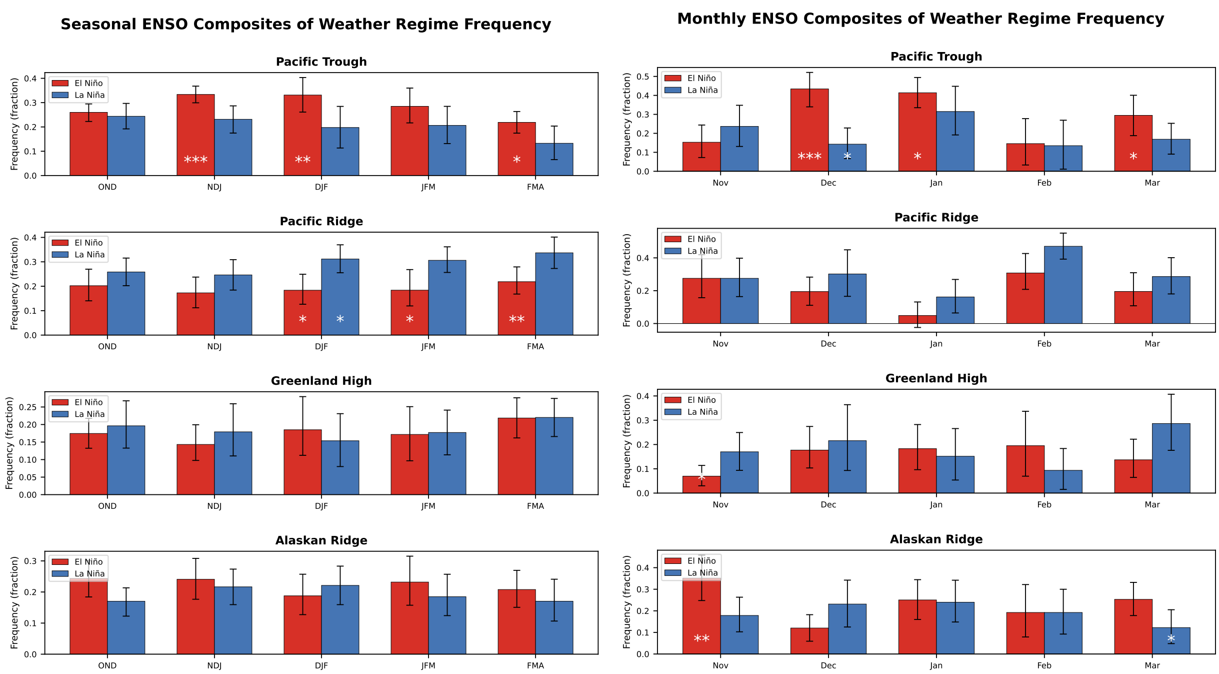

FIG. 8: Seasonal (left column) and monthly (right column) ENSO composites of weather regime frequency. One, two, and three stars indicate $p < 0.05$, $p < 0.01$, and $p < 0.001$, respectively, for the statistical significance of the difference between the ENSO-conditioned weather regime frequency and the all-years frequency (two-sided permutation test of winter labels). Error bars are 95% bootstrap confidence intervals.

Another pathway by which ENSO might influence HDDs is through changes in weather-regime frequency (Straus et al. 2007). Lee et al. (2023) found on a year-round basis that during warm ENSO conditions, Pacific Trough and Alaskan Ridge are more frequent, while Pacific Ridge is less frequent. The monthly and seasonal composites of weather-regime frequency show ENSO-dependent shifts that are clearest for Pacific Trough and Pacific Ridge (Fig. 8). At seasonal resolution, Pacific Trough is more frequent during El Niño, with the NDJ, DJF, and FMA differences being statistically significant. Pacific Ridge shows the opposite ENSO dependence: it is less frequent during El Niño. The El Niño reduction in Pacific Ridge frequency is statistically significant in DJF through FMA. At monthly resolution, the El Niño-enhanced Pacific Trough frequency is statistically significant in December, January, and March, and not present in November. Alaskan Ridge is more frequent in most seasons during El Niño, but the change is not statistically significant and less robust at monthly resolution. Greenland High shows the least coherent ENSO-dependent

City		Oct	Nov	Dec	Jan	Feb	Mar
Atlanta	All	74	310	480	592	395	236
	EN	75	328	441	600	*442*	238
	LN	74	324	502	594	374	250
Boston	All	259	587	866	1029	914	773
	EN	271	584	*807*	1007	950	770
	LN	245	576	891	1026	884	771
Burbank	All	8	116	249	245	198	166
	EN	15	107	262	244	190	152
	LN	7	123	242	244	219	**214**
Chicago O'Hare	All	316	687	1022	1214	1013	744
	EN	341	712	**910**	1190	1009	731
	LN	*284*	676	1087	1206	1020	757
Cincinnati	All	256	603	836	1027	815	576
	EN	272	608	**752**	1006	859	559
	LN	239	607	890	1032	789	595
Dallas	All	52	219	428	539	387	167
	EN	61	*261*	412	558	396	191
	LN	44	200	438	532	393	163
Houston	All	19	130	265	358	216	87
	EN	15	*161*	259	375	226	98
	LN	18	117	271	350	222	90
Las Vegas	All	18	192	455	450	295	135
	EN	23	212	466	442	279	151
	LN	14	178	455	453	324	149
Minneapolis–St. Paul	All	426	831	1271	1468	1268	917
	EN	*470*	861	**1133**	1418	1237	870
	LN	390	818	*1352*	1474	1307	949
New York	All	154	461	742	908	792	629
	EN	173	464	*688*	889	*837*	611
	LN	134	451	762	898	753	632
Philadelphia	All	168	495	757	910	769	572
	EN	188	496	*699*	886	*822*	555
	LN	155	496	791	911	735	586
Portland	All	278	524	700	705	611	524
	EN	262	527	666	683	**565**	*496*
	LN	287	522	724	699	**651**	**570**
Sacramento	All	70	332	515	491	383	279
	EN	73	343	500	474	*358*	271
	LN	70	334	518	504	**416**	*316*

TABLE 2: Monthly HDD ENSO composites for the 13 cities where CME Group weather derivatives are offered: all-years (All), El Niño (EN), and La Niña (LN) means of monthly total HDDs, detrended and recentered to the most recent year. Italic indicates $p < 0.05$ and bold $p < 0.01$ for the difference from the all-years mean.

frequency changes across months and seasons, consistent with this regime being primarily linked to Atlantic, rather than Pacific, variability.

The ENSO-related shifts in Pacific Trough and Pacific Ridge frequency align broadly with the corresponding ENSO HDD composite anomalies. In December, the increased frequency of Pacific Trough during El Niño provides a plausible contribution to the negative HDD anomalies over much of the northern and eastern United States. In February, the enhanced frequency of Pacific Ridge during La Niña likewise matches the positive HDD anomalies in parts of the western United States and the negative anomalies in the East. Overall, the frequency composites are consistent with an interpretation in which ENSO affects HDDs in part through changes in the occurrence of weather regimes.

e. Station data and weather derivatives

To connect directly with weather derivative applications, we repeated some of the analysis with station data from the 13 CME cities. Based on the climate division analysis (Fig. 4), the strongest El Niño signals are expected to be reduced HDDs in Chicago and Minneapolis–St. Paul during December and in Portland during February. Indeed, December HDD reductions in those cities during El Niño are highly significant (Table 2). In addition, consistent with the division

City		Oct	Nov	Dec	Jan	Feb	Mar
Atlanta	PT	**+1.0**	-0.2	+0.1	-1.3	-1.2	-0.9
	PR	**-1.9**	**-2.7**	**-5.0**	**-6.1**	**-4.9**	**-3.2**
	GH	+0.3	-0.1	*+2.5*	*+2.8*	+2.5	*+2.4*
	AKR	+0.3	**+3.8**	**+3.4**	**+4.9**	**+3.3**	**+2.6**
Boston	PT	+1.0	-0.8	-1.0	**-2.6**	**-2.5**	-0.5
	PR	**-2.9**	**-2.5**	**-3.4**	**-4.8**	**-2.9**	**-2.9**
	GH	+1.0	**+2.4**	+1.1	**+3.3**	*+2.2*	+1.4
	AKR	+0.2	**+2.0**	**+4.2**	**+4.4**	**+3.1**	**+2.3**
Burbank	PT	-0.2	*-1.3*	-1.0	-0.5	*-1.7*	-1.2
	PR	+0.2	+0.5	**+2.1**	**+3.1**	**+3.0**	+0.9
	GH	+0.5	**+3.0**	+1.2	+1.3	+1.0	+1.4
	AKR	-0.2	-0.8	**-1.9**	**-2.2**	*-1.9*	-1.2
Chicago O'Hare	PT	-0.7	**-2.8**	**-4.9**	**-5.7**	**-6.3**	**-3.5**
	PR	**-4.3**	**-3.3**	*-3.4*	**-5.6**	*-4.1*	**-4.3**
	GH	+1.9	+2.0	+1.7	**+5.3**	+2.8	*+3.0*
	AKR	**+3.2**	**+6.8**	**+8.2**	**+9.3**	**+8.0**	**+6.5**
Cincinnati	PT	+0.5	-1.1	*-2.5*	**-4.2**	**-3.8**	**-3.0**
	PR	**-4.6**	**-3.9**	**-5.1**	**-7.1**	**-5.6**	**-4.4**
	GH	+1.4	+1.6	+2.5	**+5.0**	*+3.5*	**+3.9**
	AKR	**+2.3**	**+5.5**	**+6.7**	**+8.0**	**+6.2**	**+5.2**
Dallas	PT	-0.4	-1.2	**-2.6**	*-2.3*	**-3.6**	*-1.6*
	PR	-0.7	*-2.2*	**-3.1**	**-3.8**	*-3.1*	**-2.5**
	GH	+0.4	+0.2	+1.4	*+3.0*	*+2.9*	+0.7
	AKR	**+1.2**	**+4.5**	**+4.7**	**+4.7**	**+4.5**	**+4.1**
Houston	PT	+0.1	-0.3	-1.1	-1.2	*-1.8*	-0.9
	PR	-0.3	**-1.9**	**-3.2**	**-4.0**	**-2.8**	**-1.5**
	GH	-0.0	-0.9	+1.1	+1.2	+1.6	+0.1
	AKR	+0.3	**+3.4**	**+3.7**	**+4.3**	**+3.2**	**+2.7**
Las Vegas	PT	**-0.7**	**-2.0**	*-1.3*	*-1.4*	*-1.8*	*-1.4*
	PR	+0.4	+1.3	**+2.0**	**+1.9**	*+2.0*	+0.9
	GH	*+0.7*	+1.8	+0.6	+1.4	+1.1	+0.9
	AKR	-0.1	-0.0	-1.0	-0.5	-0.3	-0.5
Minneapolis–St. Paul	PT	**-2.6**	**-5.0**	**-7.6**	**-7.9**	**-8.5**	**-5.7**
	PR	**-3.4**	-2.3	-1.3	-2.1	-2.2	*-2.9*
	GH	*+2.6*	+3.0	+1.7	**+6.2**	+2.4	+2.1
	AKR	**+4.4**	**+7.6**	**+8.8**	**+9.5**	**+9.5**	**+8.2**
New York	PT	+0.9	-0.8	-1.2	**-2.7**	**-2.8**	-0.9
	PR	**-2.9**	**-2.8**	**-3.7**	**-5.0**	**-3.4**	**-2.9**
	GH	+0.8	*+1.8*	+1.7	*+3.1*	*+2.8*	+1.8
	AKR	+0.6	**+2.8**	**+4.5**	**+5.0**	**+3.4**	**+2.5**
Philadelphia	PT	*+1.2*	-0.5	-1.2	*-2.6*	**-2.6**	-1.4
	PR	**-3.4**	**-3.0**	**-3.9**	**-5.2**	**-4.0**	**-3.0**
	GH	+0.9	*+1.9*	+1.9	*+3.2*	*+3.0*	*+2.4*
	AKR	+0.6	**+3.0**	**+4.5**	**+5.2**	**+3.5**	**+2.8**
Portland	PT	-0.9	**-2.4**	**-3.4**	**-2.7**	**-2.9**	*-1.1*
	PR	**+1.7**	+1.1	+1.5	+1.2	*+1.9*	**+2.0**
	GH	+1.1	+1.6	+1.0	+1.5	+0.6	+0.8
	AKR	*-1.6*	+1.0	**+2.3**	**+2.0**	+1.1	**-1.4**
Sacramento	PT	-0.5	*-1.6*	*-1.5*	**-1.5**	*-1.1*	-0.9
	PR	+0.6	*+1.7*	*+1.6*	**+2.0**	**+1.8**	*+1.3*
	GH	*+0.9*	+1.2	-0.3	+0.6	+0.5	*+1.5*
	AKR	-0.7	-0.5	+0.7	+0.2	-0.5	**-1.6**

PT	Pacific Trough	PR	Pacific Ridge
GH	Greenland High	AKR	Alaskan Ridge

TABLE 3: Weather regime composite anomalies by month of daily HDDs in the 13 cities where CME Group weather derivatives are offered. Italic indicates $p < 0.05$ and bold $p < 0.01$.

composites, December HDD reductions in Boston, Cincinnati, New York, and Philadelphia are also statistically significant. While the December La Niña composites have higher HDDs than El Niño at these cities, only the Minneapolis–St. Paul La Niña increase is statistically significant. For the West Coast February El Niño signal, Sacramento joins Portland in having significantly lower HDDs. The February El Niño HDD division composites (Fig. 4) show elevated HDDs on the East Coast and into the Southeast, and this pattern is reflected in higher-than-average February HDDs in Atlanta, New York, and Philadelphia. The expected February–March La Niña increase in West Coast HDDs is present and statistically significant in Portland and Sacramento. The weak November HDD increase seen in the division data during El Niño is also present in the station data for several cities. Statistically significant reductions in December daily HDD IQR are present during El Niño in Chicago, Cincinnati, Dallas, and Minneapolis–St. Paul (Table S1). Statistical significance in November–March and December–February HDD ENSO composites is limited to El Niño for Chicago (DJF only) and Minneapolis–St. Paul, and to La Niña for Portland and Sacramento (Table S2).

City		Oct	Nov	Dec	Jan	Feb	Mar
Atlanta	PT	*+2.0*	-1.4	**-3.0**	-0.4	-1.5	-0.8
	PR	**-4.5**	-0.9	+0.6	+1.2	-0.7	**-2.7**
	GH	+0.1	+0.4	+1.3	-0.8	+0.8	-0.9
	AKR	-0.1	+0.3	-1.7	-0.4	-1.5	+0.2
Boston	PT	+1.1	-1.3	-0.5	*-2.6*	-1.0	-0.8
	PR	+0.0	+0.4	-0.8	-0.6	+0.1	+1.0
	GH	*-2.2*	*-2.1*	-0.7	-1.2	-2.3	*-2.2*
	AKR	+0.6	-0.7	+0.1	-1.1	-0.6	*+2.0*
Burbank	PT	+0.0	-0.9	-1.6	-1.2	+0.5	-0.2
	PR	+0.0	+0.0	+0.1	-1.8	+1.0	+0.1
	GH	+1.7	+0.3	*-2.0*	-1.6	-1.5	-0.1
	AKR	-0.3	-1.3	+0.1	-0.9	+1.1	-1.6
Chicago O'Hare	PT	-0.4	+0.0	**-5.3**	**-5.6**	**-4.7**	+1.7
	PR	*-2.5*	-1.8	-1.7	-1.8	-2.8	+1.9
	GH	+0.2	+0.4	+1.0	-1.7	+0.1	*-3.5*
	AKR	-1.0	+2.1	+0.2	-0.3	-1.9	+2.1
Cincinnati	PT	-0.9	*-2.2*	**-4.6**	**-3.9**	*-2.8*	+1.2
	PR	**-4.7**	-1.5	+1.3	-1.0	-0.1	-1.3
	GH	-0.7	-1.7	+1.0	-1.2	+0.8	*-3.4*
	AKR	-0.3	-1.0	-1.9	-1.0	-1.5	+0.4
Dallas	PT	-0.1	-0.4	**-3.4**	**-2.7**	**-3.3**	*-2.2*
	PR	-1.8	*-2.0*	+1.4	+1.0	+2.0	**-2.7**
	GH	+0.9	-1.5	+2.1	+0.1	+1.2	+0.5
	AKR	*+2.0*	+1.1	-1.0	+0.7	+1.3	**+3.8**

PT Pacific Trough PR Pacific Ridge
GH Greenland High AKR Alaskan Ridge

City		Oct	Nov	Dec	Jan	Feb	Mar
Houston	PT	+0.0	+0.1	**-3.6**	-1.4	*-2.2*	-1.2
	PR	+0.1	**-4.3**	-2.1	+0.3	**-3.7**	**-3.1**
	GH	+0.0	-1.0	+1.9	+1.1	+1.2	+0.4
	AKR	+0.0	**+4.4**	-1.5	-0.7	+1.7	**+4.1**
Las Vegas	PT	-0.2	-0.2	**-1.9**	-0.9	-1.0	**-2.1**
	PR	*+1.3*	-0.3	+1.3	+0.3	+0.2	+0.8
	GH	+1.2	-1.0	-0.3	*-1.4*	-0.0	+0.8
	AKR	+0.0	-1.1	-0.4	+0.5	+1.3	-0.8
Minneapolis–St. Paul	PT	-1.4	-0.3	**-8.4**	**-7.4**	**-7.6**	-1.9
	PR	+0.1	-0.9	-2.4	-3.0	-3.2	-0.9
	GH	-1.0	-1.2	-0.7	-2.7	-1.0	-2.8
	AKR	-2.2	-0.0	-1.5	-2.2	*-4.1*	**+4.0**
New York	PT	+0.3	*-1.4*	-1.4	*-2.3*	-1.3	-0.8
	PR	**-3.0**	-1.1	-0.8	*-3.0*	+0.1	+0.9
	GH	-0.8	-1.4	-0.5	-0.6	*-2.5*	-1.7
	AKR	+1.0	-0.1	+0.0	-0.4	+0.7	**+2.3**
Philadelphia	PT	+0.2	-1.4	**-2.7**	**-3.2**	**-2.3**	-0.9
	PR	**-3.6**	-0.9	-0.8	-1.3	-0.3	+1.1
	GH	-1.2	-1.2	+0.2	-1.3	*-2.7*	*-2.9*
	AKR	+0.7	-0.1	+0.1	-0.4	-0.8	+0.6
Portland	PT	-0.6	+0.0	-0.4	*-1.5*	**-1.8**	*-1.0*
	PR	-1.1	-0.9	-0.4	+0.2	-0.7	-0.0
	GH	+1.5	+0.3	-1.4	+0.2	-0.7	-0.5
	AKR	+0.9	+1.0	+1.0	-0.6	**+2.8**	*+1.4*
Sacramento	PT	-0.8	+0.5	-0.6	+0.1	*-1.4*	-1.2
	PR	+0.7	-0.8	+0.1	-0.1	+0.5	+1.0
	GH	+1.3	+0.2	-1.1	-0.3	-1.1	-1.2
	AKR	**-2.2**	+0.4	+1.0	+0.1	+1.1	-0.7

TABLE 4: Weather regime composite anomalies by month of daily HDD IQR in the 13 cities where CME Group weather derivatives are offered. Italic indicates $p < 0.05$ and bold $p < 0.01$.

As in the division-level analysis (Fig. 6), weather regime HDD composites in CME station data are larger, more systematic, and more consistent than the ENSO ones (Table 3). Pacific Trough is associated with negative HDD anomalies at most stations. November–March HDD anomalies are negative in all cities except Atlanta. The negative HDD signal is particularly clear at Chicago O'Hare and Minneapolis–St. Paul, where HDD anomalies are negative and highly significant ($p < 0.01$) in all months from November through March. Boston, Cincinnati, New York, and Philadelphia also have highly significant negative Pacific Trough anomalies in January and February. Pacific Ridge shows an east-west dipole in the division-level analysis with strong negative anomalies in the east and more modest positive ones in the west. This pattern is reproduced in the station data. The four western cities (Burbank, Las Vegas, Portland, and Sacramento) have positive HDD anomalies in all months, while the other cities have negative HDD anomalies in all months, with many being highly significant. Greenland High days are associated with positive HDD anomalies present in nearly all CME stations and months, matching the division-level analysis. In division data, Alaskan Ridge days are associated with positive HDD anomalies over the central and eastern United States and weakly negative anomalies in the West. Station anomalies are likewise positive, seasonally consistent, and mostly highly significant at the nine non-western cities. The four western cities are more mixed: Burbank and Las Vegas are mostly negative, Portland is positive in December and January, and Portland and Sacramento are negative in March. The weather regime signal in daily IQR is mostly sporadic except for Pacific Trough, which reduces the daily IQR (Table 4) in all the eastern cities during December–February, with the Pacific Trough IQR reductions in Chicago, Dallas, Minneapolis–St. Paul, and Philadelphia being substantial and highly significant.

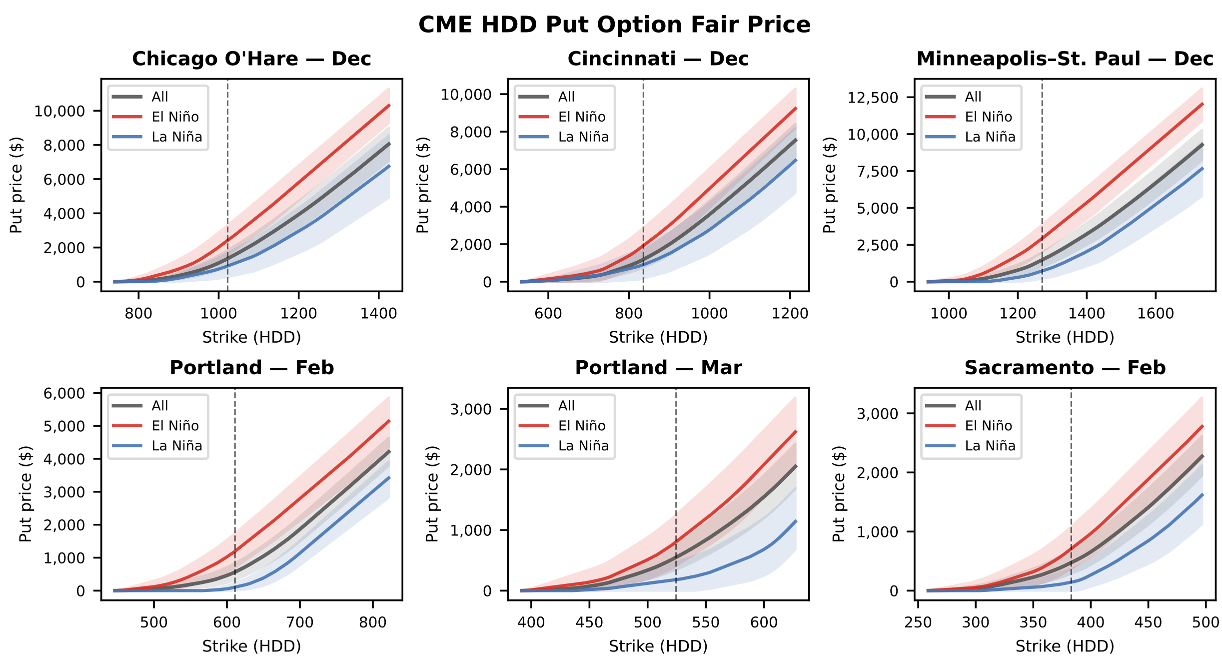

FIG. 9: Put option prices plotted as a function of strike and ENSO phase. The range of strike values matches the HDD range of the city and month. The dotted line indicates the climatological at-the-money (C-ATM) strike. Shading is 95% bootstrap percentile bands.

To translate the ENSO-related changes in mean and spread of HDDs into a quantity directly relevant to weather derivative markets, we computed ENSO-conditioned fair values of put options as functions of strike for six CME city–month cases with highly significant ENSO HDD composite anomalies (Fig. 9). Burbank was excluded due to its shorter station data record. Put options pay out if the observed HDD is less than the strike and thus provide mild-winter protection. Put-option fair prices decrease monotonically as the strike decreases, approaching zero as the strike reaches the historical HDD minimum, and the ENSO differences become small. The ENSO separation in put prices tends to increase with increasing strike until a point above which the price curves are approximately linear and have the same slopes. The reason for this linear behavior at high strikes is that most observed HDD values fall below the strike, and the price is therefore proportional to the difference between the strike and the all-cases average HDD value. For the December Midwest and Northeast cases, El Niño prices are higher than the all-years and La Niña prices. The Chicago and Minneapolis–St. Paul El Niño price curves are notable for their clear separation from the all-years and La Niña curves for strikes above the climatological mean. La Niña put-option prices for Portland in February and March and for Sacramento in February are lower than El Niño ones, consistent with the La Niña tendency toward lower HDDs in the Pacific Northwest and parts of the western United States.

f. ENSO teleconnection

A notable feature of the ENSO HDD composites and ENSO-conditioned weather-regime frequencies is the unusually strong El Niño signal in December, which is not matched in other months or during La Niña. To examine whether this month dependence reflects corresponding changes in the large-scale circulation, we computed composites of eddy (zonal mean removed) 200-hPa geopotential height. Removing the zonal mean emphasizes the regional ridges and troughs that form the Rossby-wave train linking the tropical Pacific and North America. From December through March, the composites show broadly similar wave-train structures, with El Niño characterized approximately by a ridge–trough–ridge sequence across the North Pacific–North American sector and La Niña by the opposite-signed pattern (Fig. 10). The El Niño downstream ridge is dynamically consistent with the broad warming and reduced HDDs over the central and eastern United States. The amplitude and precise location of the anomaly centers, however, vary from month to month. The December El Niño composite stands out because the wave train is strong and spatially coherent, with a pronounced North Pacific trough and downstream ridge over eastern North America. In January through March, the El Niño anomaly centers are generally weaker, less spatially extensive, or displaced relative to North America. La Niña broadly reverses the El Niño wave pattern with differences in amplitude. These amplitude differences are not consistent across months: the La Niña amplitude is weaker in December and January but stronger than El Niño in February and March. While the largest La Niña anomalies occur in January and February, with a strong North Pacific ridge, their downstream structure is less favorably positioned to produce a broad HDD response beyond the western United States. October and November differ from the subsequent cold-season months: the height anomalies over northern North America tend to have the opposite sign from their December counterparts, in agreement with the corresponding reversal seen in the November HDD composites. Consistent with the lack of HDD asymmetry, the El Niño–La Niña eddy 200-hPa geopotential height asymmetry is not statistically significant (Fig. S5).

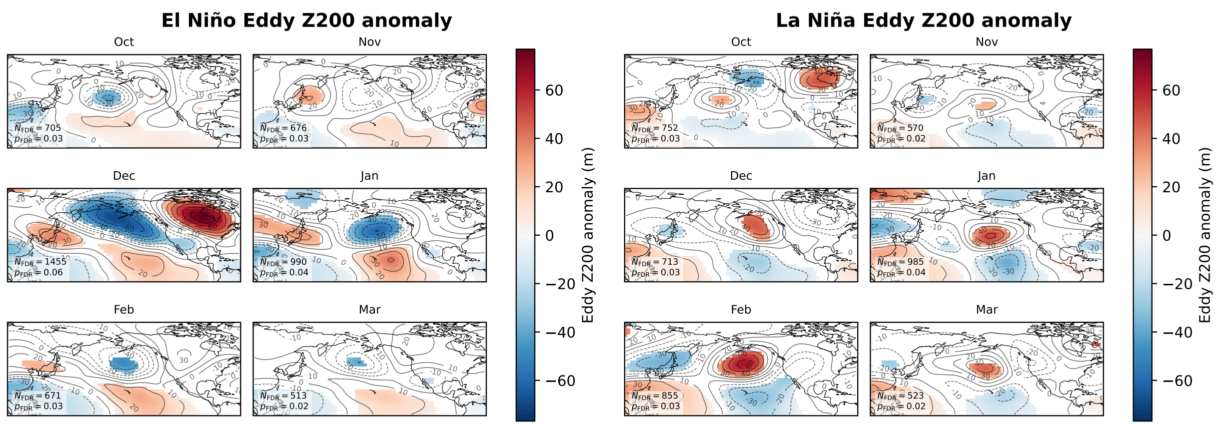

FIG. 10: Monthly ENSO composites of detrended eddy 200 hPa geopotential height (Z200) anomalies October–March.

4. Summary and discussion

Although the 1997–98 El Niño event played a pivotal role in the birth of the U.S. market for heating degree day (HDD)-based weather derivatives nearly three decades ago, few if any published studies have quantified the relation of U.S. HDDs with ENSO. Here we addressed this gap by computing ENSO composite anomalies of cold-season HDDs for 16 El Niño and 16 La Niña events over the period 1979–2026. In addition, we considered the relation of ENSO and HDDs with North American weather regimes, which are widely used in the energy industry to summarize synoptic weather patterns. We designed our analysis to align with weather-derivative applications. Namely, HDDs were analyzed at monthly resolution (November–March) to match the shortest contract periods, values were detrended and recentered to present, and station data from cities where the CME Group offers weather derivatives were analyzed in addition to spatially resolved NOAA climate-division data.

Overall, ENSO composites of NOAA division-level data show the expected large-scale negative HDD anomalies during El Niño and positive HDD anomalies during La Niña (Fig. 4). The strongest signal is the December El Niño reduction in HDDs in the Midwest and Northeast. El Niño HDD anomalies are weaker in other cold-season months and have the opposite sign in November. HDD increases during La Niña conditions are weaker than the El Niño ones and are statistically significant only in March. At the station level, the December El Niño HDD reductions in Chicago, Cincinnati, and Minneapolis–St. Paul, along with February La Niña HDD increases in Portland and Sacramento, are notably strong and robust (Table 2).

Because North American daily temperature variability is reduced during El Niño winters (Becker and Tippett 2024; Martineau et al. 2021; Smith and Sardeshmukh 2000), we also examined ENSO composites of the within-month interquartile range (IQR) of daily HDDs. The clearest ENSO signal in HDD variability is the December El Niño reduction of the daily HDD IQR over much of the central United States (Fig. 4). At the station level, the December El Niño IQR reductions are statistically significant in Chicago, Cincinnati, Dallas, and Minneapolis–St. Paul (Table S1). A physical explanation for this reduction in variability is essentially the same as that used to explain how Arctic amplification of global warming reduces midlatitude temperature variability, namely that El Niño warming in the northern part of North America reduces the meridional temperature gradient, which in turn reduces advection-generated temperature variance (Schneider et al. 2015).

We examined North American weather regimes, which operate on subseasonal time scales, to see whether they provide a pathway for the ENSO signal. Independent of ENSO, weather regimes have spatially coherent and statistically robust relations with monthly HDDs in all cold-season months (Fig. 6). Both Greenland High and Alaskan Ridge are associated with HDD increases. HDD increases east of the Rockies are statistically significant during Alaskan Ridge days November–March, while statistically significant Greenland High HDD increases are limited to January. Pacific Trough and Pacific Ridge HDD composites seem relevant for ENSO, which reflects their being linked to Pacific rather than Atlantic variability. The HDD decrease pattern during Pacific Trough days closely resembles the December El Niño HDD decrease and, like it, is accompanied by a decrease in daily HDD variability (Fig. 7). The positive HDD anomalies on the west coast during Pacific Ridge days resemble the late-winter La Niña HDD signal. When we examined the influence of ENSO weather regime frequency and intensity, we found the largest impacts were in frequency (Fig. 8). El Niño increases the frequency of Pacific Trough (largest increase in December) and decreases the frequency of Pacific Ridge (largest decrease in February). The increased Pacific

Trough frequency during El Niño is consistent with the December El Niño HDD reduction over much of the northern and eastern United States. Likewise, the increased February–March frequency of Pacific Ridge during La Niña, though not statistically significant, is consistent with the late-winter La Niña HDD increases in the western United States. Within-regime ENSO anomalies are mostly small and not statistically significant (Figs. S3, S4), which means that the primary ENSO impact is to change the frequency of the regimes rather than their HDD signatures.

Weather derivative option-price calculations further translate the ENSO HDD signals into financially relevant quantities. For the city–month pairs with the strongest ENSO HDD signals, ENSO-conditioned fair put prices differ from the all-years prices in the expected direction over a wide range of strikes (Fig. 9). The separation is clearest for Chicago and Minneapolis–St. Paul in December, where the El Niño reductions in both the mean and the variability of HDDs act together to raise the fair value of put options.

A long-standing question in ENSO studies is whether ENSO teleconnections substantially differ between warm and cool phases. Addressing this issue using observations is challenging due to the small number of ENSO events in the well-observed historical record and the modest size of the ENSO signals compared to internal variability (Deser et al. 2017). Here we found notable differences between El Niño and La Niña HDD composites. For instance, El Niño HDD composite anomalies are statistically significant in December and February, while La Niña anomalies are not. In March, the opposite is true, with La Niña HDD composite anomalies being statistically significant and El Niño anomalies not (Fig. 4). Similar results for El Niño and La Niña HDD composites are also present in the station data (Table 2). In these cases, statistical significance conclusions reflect stronger signals or reduced variability, and therefore indicate differences between warm and cool teleconnections. Despite these differences in statistical significance, the only statistically significant asymmetry detected is the El Niño DJF reduction in IQR (Fig. S2). Previous studies have often assessed ENSO asymmetry using the sum of El Niño and La Niña composite anomalies relative to the all-winter climatology. Our neutral-centered test more directly addresses the question of equal-and-opposite responses, incorporates uncertainty in the El Niño, La Niña, and neutral means, and is a stricter test with less power. No asymmetries were detected in either the HDD composites (Fig. S2) or the eddy 200-hPa height composites (Fig. S5). This finding is a reminder that differences in statistically significant patterns do not imply statistically significant differences.

The failure to detect ENSO asymmetry here may well be due to the small sample size (16 warm and cool winters) in the asymmetry analysis and the resulting lack of statistical power. The asymmetry results here agree with Deser et al. (2018), who found that El Niño North American DJF surface temperature responses were stronger than La Niña ones but that the difference was mostly not statistically significant (10% level; their Fig. 12). Our results differ from their detection of FMA asymmetries (their Fig. S10), perhaps due to different ENSO events being analyzed, a less stringent significance level, or lack of false discovery rate control. Hoerling et al. (1997) did find statistically significant asymmetries in DJF North American surface temperature composites in nine El Niño and nine La Niña events over the period 1950–1996.

Another notable finding here is the concentration of El Niño impacts in December. ENSO impacts are typically analyzed at seasonal resolution. However, the choice of seasonal resolution involves a trade-off: when a signal persists over several months, seasonal averaging does reduce noise, but if the signal genuinely varies from month to month, seasonal averaging dilutes and obscures within-season variations. Comparing the monthly and seasonal ENSO HDD composites here demonstrates that a seasonal signal does not imply similar signals in the months that comprise the season. A more difficult question is whether the monthly dependence, and the December concentration in particular, reflects sampling variability or a physical mechanism that is expected to be seen in independent data. A few studies have examined subseasonal variability in ENSO teleconnections. Chapman et al. (2021) found monthly modulation of potential predictability over North America in an ENSO-forced atmospheric model. Bladé et al. (2008) found a December to January shift in the sensitivity of the North Pacific circulation to tropical forcing related to subseasonal changes in the mean state, while Kim et al. (2018) connected such circulation seasonality to changes in forcing amplitudes. Jong et al. (2016) found that the ENSO influence on California precipitation strengthens from early to late winter. Park et al. (2023) found a substantial weakening of the ENSO teleconnections to western North America in mid-winter (January), not unlike the weakening seen here, and related it to convection over the equatorial Indian Ocean.

The findings here suggest several directions for future work. Regression-based approaches might improve on the HDD composite analysis by accounting for ENSO amplitude, making fuller use of the record, and including warm/cool asymmetry via piecewise linear formulations (Becker and Tippett 2024; Frankignoul and Kwon 2022; Hoerling et al. 2001). Similar analysis could examine whether the December concentration of the El Niño signal appears in other variables, such as precipitation. Analysis using model simulations or forecasts could remove the sample size limitation of observational studies, though model biases cannot be ignored. The skill with which HDDs can be predicted based on expected ENSO conditions (Tippett and Becker 2026) or current subseasonal-to-seasonal forecast systems could be assessed.

Acknowledgments. Support from NSF is acknowledged by EJB (2223262). The authors thank Tim Boyce (TP ICAP), Todd Crawford (Atmospheric G2), Nicholas Ernst (BGC Financial), and Tom Paylor (Munich Re Trading LLC) for their useful comments. The authors acknowledge the use of AI tools, including OpenAI's ChatGPT and Anthropic's Claude, to assist with code and manuscript editing. The scientific results and conclusions, as well as any views or opinions expressed herein, are those of the authors and do not necessarily reflect the views of NWS, NOAA, or the Department of Commerce.

Data availability statement. NClimDiv (Vose et al. 2014b) and nClimGrid-Daily (Durre et al. 2022b) data are openly available from the NOAA National Centers for Environmental Information `https://www.ncei.noaa.gov`. CPC ONI data are openly available from the NOAA Climate Prediction Center `https://www.cpc.ncep.noaa.gov/products/analysis_monitoring/enso/oni/v5/`. Weather regime classifications are available in the Zenodo archive `https://doi.org/10.5281/zenodo.21971083`. ERA5 data were downloaded from the Climate Data Store (CDS) `https://cds.climate.copernicus.eu/`.

References

Arguez, A., A. Inamdar, M. A. Palecki, C. J. Schreck, and A. H. Young, 2019: ENSO normals: A new US climate normals product conditioned by ENSO phase and intensity and accounting for secular trends. *Journal of Applied Meteorology and Climatology*, **58**, 1381–1397.

Barnston, A. G., M. H. Glantz, and Y. He, 1999: Predictive skill of statistical and dynamical climate models in SST forecasts during the 1997-98 El Niño Episode and the 1998 La Niña Onset. *Bull. Amer. Meteor. Soc.*, **80**, 217–243.

Becker, E. J., and M. K. Tippett, 2024: Impact of ENSO and trends on the distribution of North American wintertime daily temperature. *Journal of Climate*, **37**, 3509–3520, https://doi.org/10.1175/JCLI-D-23-0569.1.

Bladé, I., M. Newman, M. A. Alexander, and J. D. Scott, 2008: The late fall extratropical response to ENSO: Sensitivity to coupling and convection in the tropical west Pacific. *Journal of Climate*, **21**, 6101–6118, https://doi.org/10.1175/2008JCLI1612.1.

Campbell, S. D., and F. X. Diebold, 2005: Weather forecasting for weather derivatives. *Journal of the American Statistical Association*, **100**, 6–16.

Chapman, W. E., A. C. Subramanian, S.-P. Xie, M. D. Sierks, F. M. Ralph, and Y. Kamae, 2021: Monthly modulations of ENSO teleconnections: Implications for potential predictability in North America. *Journal of Climate*, **34**, 5899–5921, https://doi.org/10.1175/JCLI-D-20-0391.1.

Considine, G., 2000: Introduction to weather derivatives. White paper, Weather Derivatives Group, Aquila Energy, 1–10 pp.

Cook, A. R., L. M. Leslie, D. B. Parsons, and J. T. Schaefer, 2017: The impact of El Niño–Southern Oscillation (ENSO) on winter and early spring US tornado outbreaks. *Journal of Applied Meteorology and Climatology*, **56**, 2455–2478.

Cook, A. R., and J. T. Schaefer, 2008: The Relation of El Niño–Southern Oscillation (ENSO) to Winter Tornado Outbreaks. *Mon. Wea. Rev.*, **136**, 3121–3137, https://doi.org/10.1175/2007MWR2171.1.

Deser, C., I. R. Simpson, K. A. McKinnon, and A. S. Phillips, 2017: The Northern Hemisphere extratropical atmospheric circulation response to ENSO: How well do we know it and how do we evaluate models accordingly? *Journal of Climate*, **30**, 5059–5082, https://doi.org/10.1175/JCLI-D-16-0844.1.

Deser, C., I. R. Simpson, A. S. Phillips, and K. A. McKinnon, 2018: How well do we know ENSO's climate impacts over North America, and how do we evaluate models accordingly? *Journal of Climate*, **31**, 4991–5014, https://doi.org/10.1175/JCLI-D-17-0783.1.

Durre, I., A. Arguez, C. J. Schreck III, M. F. Squires, and R. S. Vose, 2022a: Daily high-resolution temperature and precipitation fields for the contiguous United States from 1951 to present. *Journal of Atmospheric and Oceanic Technology*, **39**, 1837–1855, https://doi.org/10.1175/JTECH-D-22-0024.1.

Durre, I., M. F. Squires, R. S. Vose, A. Arguez, W. S. Gross, J. R. Rennie, and C. J. Schreck, 2022b: NOAA nClimGrid-Daily Version 1 – Daily gridded temperature and precipitation for the Contiguous United States since 1951. NOAA National Climatic Data Center, URL https://doi.org/10.25921/c4gt-r169, accessed 19 August 2026, https://doi.org/10.25921/c4gt-r169.

Frankignoul, C., and Y.-O. Kwon, 2022: On the statistical estimation of asymmetrical relationship between two climate variables. *Geophysical Research Letters*, **49**, e2022GL100 777.

Halpert, M. S., and C. F. Ropelewski, 1992: Surface temperature patterns associated with the Southern Oscillation. *Journal of Climate*, **5**, 577–593, https://doi.org/10.1175/1520-0442(1992)005<0577:STPAWT>2.0.CO;2.

Hersbach, H., and Coauthors, 2020: The ERA5 global reanalysis. *Quarterly Journal of the Royal Meteorological Society*, **146**, 1999–2049, https://doi.org/10.1002/qj.3803.

Hoerling, M. P., A. Kumar, and T. Xu, 2001: Robustness of the nonlinear climate response to ENSO's extreme phases. *Journal of Climate*, **14**, 1277–1293, https://doi.org/10.1175/1520-0442(2001)014<1277:ROTNCR>2.0.CO;2.

Hoerling, M. P., A. Kumar, and M. Zhong, 1997: El Niño, La Niña, and the nonlinearity of their teleconnections. *Journal of Climate*, **10**, 1769–1786, https://doi.org/10.1175/1520-0442(1997)010<1769:ENOLNA>2.0.CO;2.

Jewson, S., and A. Brix, 2005: *Weather derivative valuation: the meteorological, statistical, financial and mathematical foundations*. Cambridge University Press.

Jong, B.-T., M. Ting, and R. Seager, 2016: El Niño's impact on California precipitation: Seasonality, regionality, and El Niño intensity. *Environmental Research Letters*, **11**, 054 021, https://doi.org/10.1088/1748-9326/11/5/054021.

Kim, S., H.-Y. Son, and J.-S. Kug, 2018: Relative roles of equatorial central Pacific and western North Pacific precipitation anomalies in ENSO teleconnection over the North Pacific. *Climate Dynamics*, **51**, 4345–4355, https://doi.org/10.1007/s00382-017-3779-6.

Lee, S., J. Furtado, and A. Charlton-Perez, 2019: Wintertime North American weather regimes and the Arctic stratospheric polar vortex. *Geophysical Research Letters*, **46**, 14 892–14 900, https://doi.org/10.1029/2019GL085592.

Lee, S. H., and L. M. Polvani, 2026: Increasing frequency and persistence of the summertime Greenland High regime not captured by a seasonal prediction model very large ensemble. *Geophysical Research Letters*, **53**, e2025GL119 421, https://doi.org/10.1029/2025GL119421.

Lee, S. H., M. K. Tippett, and L. M. Polvani, 2023: A new year-round weather regime classification for North America. *Journal of Climate*, **36**, 7091–7108, https://doi.org/10.1175/JCLI-D-23-0214.1.

Martineau, P., H. Nakamura, and Y. Kosaka, 2021: Influence of ENSO on North American subseasonal surface air temperature variability. *Weather and Climate Dynamics*, **2**, 395–412, https://doi.org/10.5194/wcd-2-395-2021.

McPhaden, M. J., 1999: Genesis and evolution of the 1997-98 El Niño. *Science*, **283**, 950–954, https://doi.org/10.1126/science.283.5404.950.

Millin, O. T., J. C. Furtado, and C. Malloy, 2024: The impact of North American winter weather regimes on electricity load in the central United States. *npj Climate and Atmospheric Science*, **7**, 254, https://doi.org/10.1038/s41612-024-00803-1.

Molina, M. J., J. H. Richter, A. A. Glanville, K. Dagon, J. Berner, A. Hu, and G. A. Meehl, 2023: Subseasonal representation and predictability of North American weather regimes using cluster analysis. *Artificial Intelligence for the Earth Systems*, **2**, e220 051, https://doi.org/10.1175/AIES-D-22-0051.1.

Park, C.-H., J. Choi, S.-W. Son, D. Kim, S.-W. Yeh, and J.-S. Kug, 2023: Sub-seasonal variability of ENSO teleconnections in Western North America and its prediction skill. *Journal of Geophysical Research: Atmospheres*, **128**, e2022JD037 985, https://doi.org/10.1029/2022JD037985.

Pérez-Carrasquilla, J. S., M. J. Molina, K. J. Mayer, K. Dagon, J. T. Fasullo, and I. R. Simpson, 2025: Observed and modeled amplification of the frequency, duration, and extreme heat impacts of the Pacific trough regime. *Earth's Future*, **13**, e2025EF007 140, https://doi.org/10.1029/2025EF007140.

Robertson, A. W., N. Vigaud, J. Yuan, and M. K. Tippett, 2020: Towards identifying subseasonal forecasts of opportunity using North American weather regimes. *Mon. Wea. Rev.*, **148**, 1861–1875, https://doi.org/10.1175/MWR-D-19-0285.1.

Ropelewski, C. F., and M. S. Halpert, 1986: North American precipitation and temperature patterns associated with the El Niño/Southern Oscillation (ENSO). *Monthly Weather Review*, **114**, 2352–2362, https://doi.org/10.1175/1520-0493(1986)114<2352:NAPATP>2.0.CO;2.

Rouges, E., M. Kretschmer, and T. G. Shepherd, 2025: On the link between weather regimes and energy shortfall during winter for 28 European countries. *Meteorological Applications*, **32**, e70 077.

Schneider, T., T. Bischoff, and H. Płotka, 2015: Physics of changes in synoptic midlatitude temperature variability. *Journal of Climate*, **28**, 2312–2331.

Smith, C. A., and P. D. Sardeshmukh, 2000: The effect of ENSO on the intraseasonal variance of surface temperatures in winter. *International Journal of Climatology: A Journal of the Royal Meteorological Society*, **20 (13)**, 1543–1557, https://doi.org/10.1002/1097-0088(20001115)20:13<1543::AID-JOC579>3.0.CO;2-A.

Straus, D. M., S. Corti, and F. Molteni, 2007: Circulation regimes: Chaotic variability versus SST-forced predictability. *Journal of Climate*, **20**, 2251–2272, https://doi.org/10.1175/JCLI4070.1.

Tippett, M. K., and E. J. Becker, 2026: ENSO-conditioned evolution of global mean surface temperature. *Geophysical Research Letters*, **53**, e2026GL124 175.

Tippett, M. K., K. Malloy, and S. H. Lee, 2024: Modulation of US tornado activity by year-round North American weather regimes. *Monthly Weather Review*, **152**, 2189–2202.

U.S. Environmental Protection Agency, 2021: Technical documentation: Heating and cooling degree days. Technical report, U.S. Environmental Protection Agency. URL https://epa.gov.

van der Wiel, K., H. C. Bloomfield, R. W. Lee, L. P. Stoop, R. Blackport, J. A. Screen, and F. M. Selten, 2019: The influence of weather regimes on European renewable energy production and demand. *Environmental Research Letters*, **14**, 094 010, https://doi.org/10.1088/1748-9326/ab38d3.

Vigaud, N., A. W. Robertson, and M. K. Tippett, 2018: Predictability of recurrent weather regimes over North America during winter from submonthly reforecasts. *Monthly Weather Review*, **146**, 2559–2577, https://doi.org/10.1175/MWR-D-18-0058.1.

Vose, R. S., and Coauthors, 2014a: Improved historical temperature and precipitation time series for US climate divisions. *Journal of Applied Meteorology and Climatology*, **53**, 1232–1251, https://doi.org/10.1175/JAMC-D-13-0248.1.

Vose, R. S., and Coauthors, 2014b: NOAA Monthly U.S. Climate Divisional Database (NClimDiv). NOAA National Climatic Data Center, accessed 19 August 2026, https://doi.org/10.7289/V5M32STR.

Supplemental material for:

ENSO, weather regimes, and U.S. heating degree days

Michael K. Tippett[a] , Emily J. Becker[b] , Simon H. Lee[c] , and Michelle L. L'Heureux[d]

[a] *Department of Applied Physics and Applied Mathematics, Columbia University, New York, New York*

[b] *Rosenstiel School of Marine, Atmospheric, and Earth Science, University of Miami, Miami, Florida*

[c] *School of Earth and Environmental Sciences, University of St Andrews, St Andrews, UK*

[d] *NOAA/NWS/NCEP/Climate Prediction Center, College Park, Maryland*

Corresponding author: Michael K. Tippett, mkt14@columbia.edu

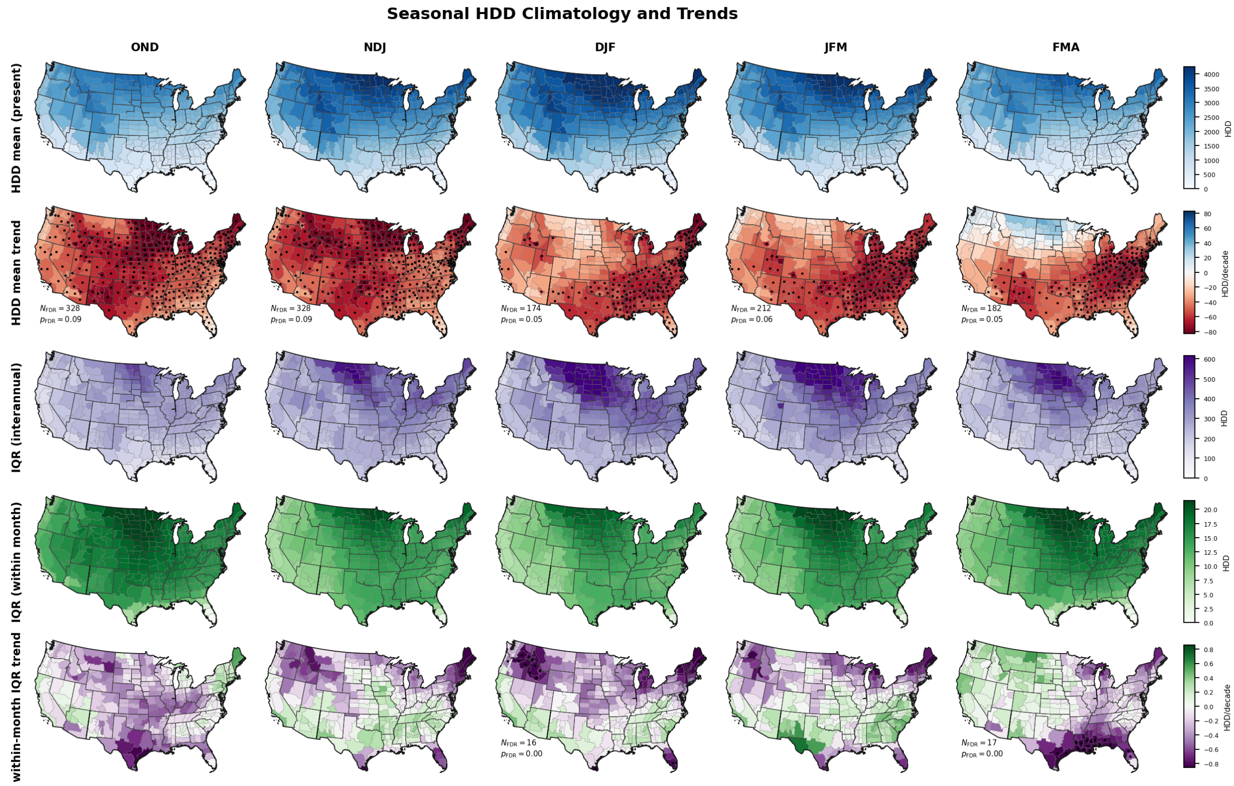

FIG. S1: October–December to February–April three-month HDD averages (top row), average trends (second row), interannual IQR of seasonal totals (third row), mean within-season daily IQR (fourth row), and within-season daily-IQR trends (bottom row).

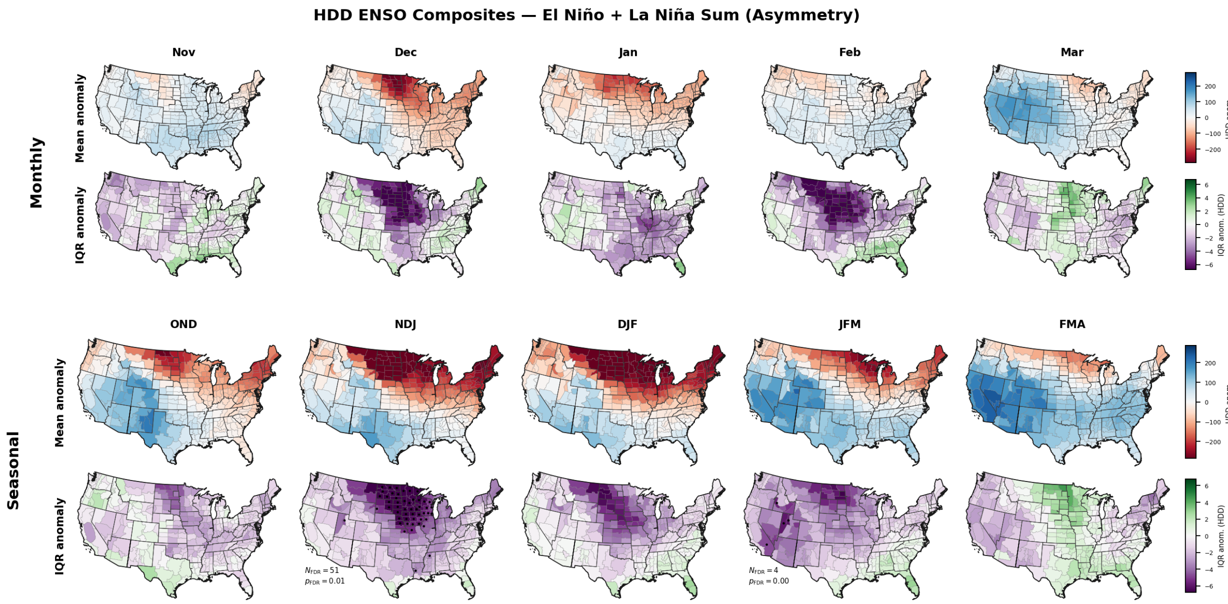

FIG. S2: Sum of monthly El Niño and La Niña HDD composite anomalies (top row) and IQR anomalies (second row). Sum of seasonal El Niño and La Niña HDD composite anomalies (third row) and IQR anomalies (bottom row).

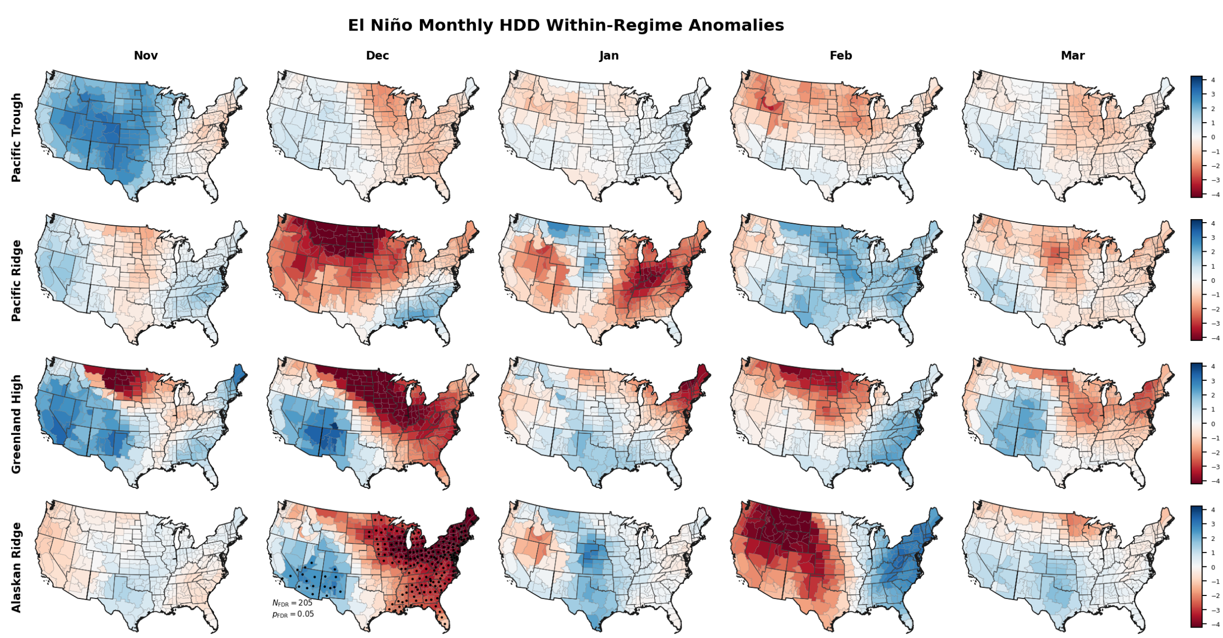

FIG. S3: November–March within-regime HDD El Niño anomalies: Average[HDD|ENSO, regime] – Average[HDD|regime].

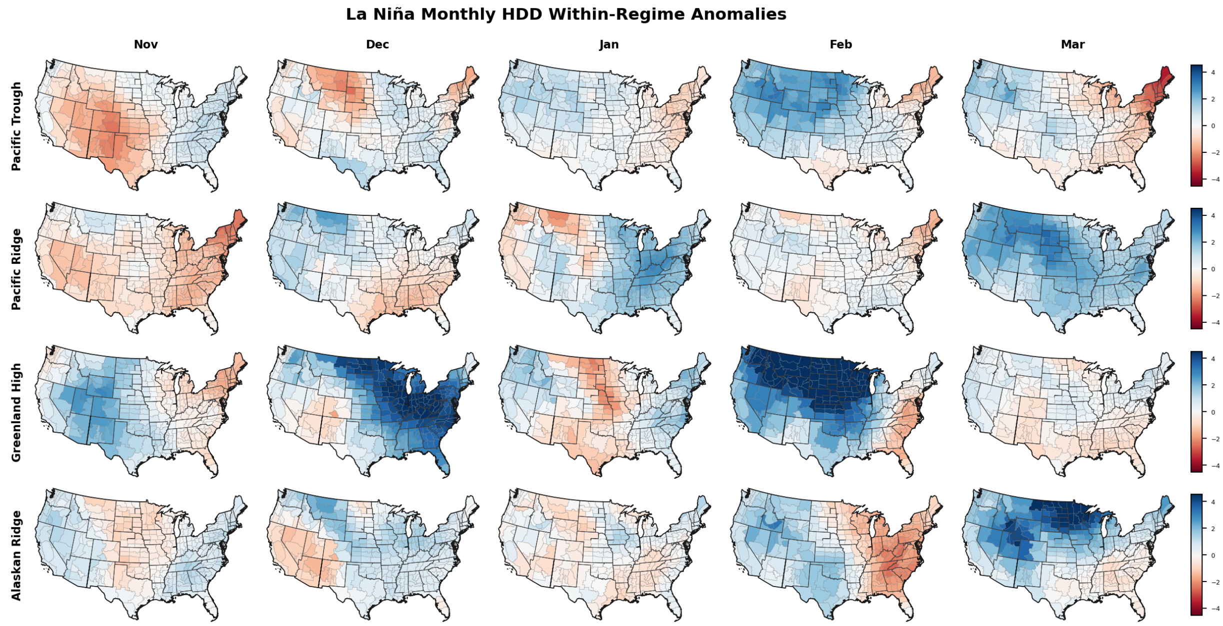

FIG. S4: November–March within-regime HDD La Niña anomalies: Average[HDD|ENSO, regime] – Average[HDD|regime].

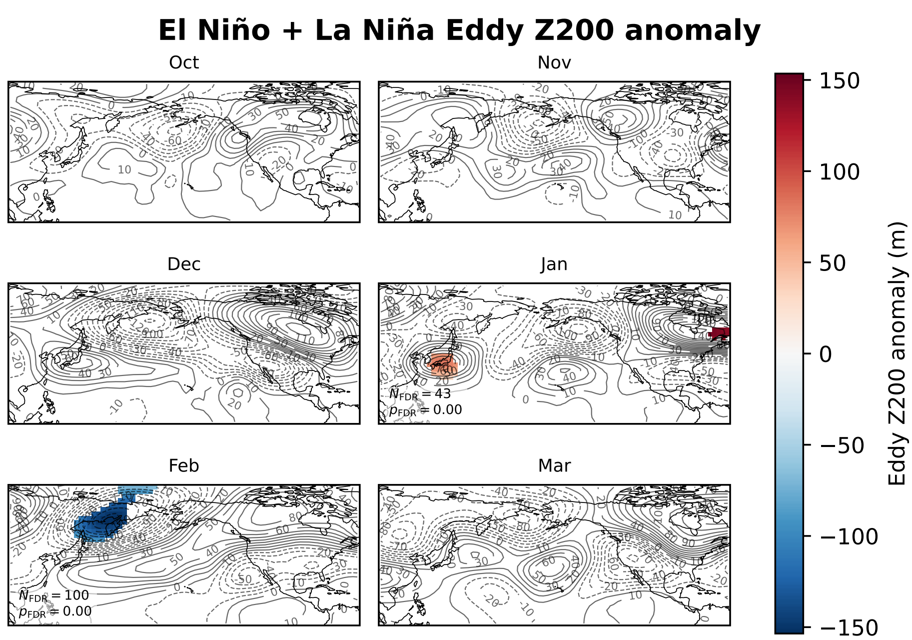

FIG. S5: Sum of monthly ENSO composites of detrended eddy 200 hPa geopotential height (Z200) anomalies October–March.

City		Oct	Nov	Dec	Jan	Feb	Mar
Atlanta	All	3	10	11	13	11	10
	EN	4	10	10	12	10	9
	LN	3	11	12	13	13	9
Boston	All	8	10	9	11	10	10
	EN	9	10	9	11	10	9
	LN	8	10	9	11	10	10
Burbank	All	0	6	5	7	7	4
	EN	0	5	5	7	*6*	4
	LN	0	6	5	7	**9**	5
Chicago O'Hare	All	13	12	12	13	12	12
	EN	12	12	**9**	13	*10*	12
	LN	13	13	13	12	14	11
Cincinnati	All	13	11	12	15	14	14
	EN	12	11	*11*	14	13	14
	LN	12	11	13	15	14	*12*
Dallas	All	2	10	11	12	15	8
	EN	2	10	*9*	12	*13*	8
	LN	1	10	12	11	*17*	8

City		Oct	Nov	Dec	Jan	Feb	Mar
Houston	All	0	7	12	12	12	4
	EN	0	8	10	11	11	4
	LN	0	7	12	13	13	4
Las Vegas	All	0	7	7	6	7	6
	EN	0	6	6	6	6	5
	LN	0	8	7	6	8	7
Minneapolis–St. Paul	All	13	13	14	18	14	12
	EN	*11*	13	**11**	18	13	13
	LN	14	*11*	14	16	15	12
New York	All	8	10	9	11	10	10
	EN	8	10	9	12	9	10
	LN	7	10	9	10	11	10
Philadelphia	All	9	9	9	11	10	11
	EN	9	9	8	11	10	10
	LN	8	9	9	10	11	10
Portland	All	6	8	6	6	5	6
	EN	7	8	6	7	*4*	7
	LN	6	7	6	6	5	6
Sacramento	All	3	7	6	5	5	6
	EN	3	6	5	5	*4*	6
	LN	4	6	5	5	6	6

TABLE S1: Monthly ENSO composites of the within-month IQR of daily HDDs for the 13 cities where CME Group weather derivatives are offered: all-years (All), El Niño (EN), and La Niña (LN) means of the per-year IQRs. Italic indicates $p < 0.05$ and bold $p < 0.01$ for the difference from the all-years mean.

	Nov–Mar (HDD)			Dec–Feb (HDD)		
City	All	El Niño	La Niña	All	El Niño	La Niña
Atlanta	2013	2048	2044	1467	1483	1470
Boston	4169	4119	4147	2809	2764	2801
Burbank	977	955	1059	692	696	705
Chicago O'Hare*	4681	4552	4745	3250	*3109*	3313
Cincinnati	3857	3784	3913	2678	2616	2711
Dallas	1740	1818	1727	1354	1366	1364
Houston	1055	1117	1050	838	859	843
Las Vegas	1528	1551	1561	1201	1187	1233
Minneapolis–St. Paul*	5755	*5519*	5900	4007	**3788**	4133
New York	3531	3489	3495	2442	2414	2413
Philadelphia	3503	3458	3520	2436	2407	2437
Portland*	3065	**2938**	*3165*	2016	**1915**	2074
Sacramento*	2001	1947	*2089*	1389	*1333*	1438

TABLE S2: All 13 CME cities; Nov–Mar and Dec–Feb strips; detrended to present. El Niño / La Niña columns: two-sided permutation test on mean ($n_{\text{perm}} = 10{,}000$); *italic* $p < 0.05$, **bold** $p < 0.01$. *City: $p<0.05$ in any strip×ENSO cell.